

國立交通大學  
光電工程研究所  
碩士學位論文

利用光纖熔拉及側耦合技術來製作長週  
期光纖光柵

Long Period Fiber Gratings by  
Fiber-Tapering and Side-Coupling



研究生：莊佩蓁

指導教授：賴暎杰

中華民國九十七年七月

# 摘要

論文名稱：利用光纖熔拉及側耦合技術來製作長週期光纖光柵

校所別：國立交通大學光電工程研究所

頁數：1 頁

畢業時間：九十六學年度第二學期

學位：碩士

研究生：莊佩蓁

指導教授：賴暎杰 老師

關鍵詞：單模的熔拉光纖、長週期光纖光柵、模態耦合、解模

在本論文中，我們利用光纖熔拉及側耦合技術來製作易於調變且高靈敏度的長週期光纖光柵。將單模光纖(SMF-28)熔拉至直徑  $20\mu\text{m}$  與鍍上金屬的長週期光柵側向接觸，利用熔拉光纖的消逝場與金屬光柵的相互作用，沿著光在光纖中傳播方向產生模態耦合，在穿透頻譜上產生帶狀的能量損失。利用外在環境的溫度與折射率變化來調變相位匹配，我們發現與一般利用單模光纖製作的光纖光柵相比，利用熔拉光纖所製作的長週期光纖光柵有相反的共振波長漂移方向。我們所得到的中心波長對折射率之調變效率( $d\lambda/dn$ )最高約為  $773\text{nm}$ ，中心波長對溫度之調變效率約為  $-0.24\text{ nm}/^\circ\text{C}$ ，與傳統光纖光柵相比(約為  $+0.06\text{ nm}/^\circ\text{C}$ )，溫度調變效率提升了四倍。因為熔拉光纖和單模光纖的色散曲線特性不同，所以擁有不同的調變趨勢和效率。

# ABSTRACT

Title : Long Period Fiber Gratings by Fiber-Tapering and Side-Coupling

Pages : 1 Page

School : National Chiao Tung University

Department : Institute of Electro-Optical Engineering

Time : July, 2008

Degree : Master

Researcher : Pei-Jhen Jhuang

Advisor : Prof. Yin-Chieh Lai

Keywords : Single mode tapered fibers 、 Long period fiber grating 、 Modal coupling 、 Mode solving

In this thesis, we experimentally demonstrate a simple LPFG structure based on fiber-tapering and side-coupling techniques to form a flexible and high-sensitivity sensing device. The LPFG is composed of a fiber taper with a uniform waist of  $20 \mu\text{m}$  in diameter and a side-contacted metal grating. The overlap of the evanescent field with the surface of metal grating leads to modal coupling along the propagation direction and provides an enhanced but opposite dip wavelength tuning tendency with respect to the temperature and refractive index change when compared to conventional LPFGs. The highest average refractive index tuning efficiency ( $d\lambda/dn$ ) is  $773 \text{ nm}$ . The average temperature tuning efficiency is estimated to be about  $-0.24 \text{ nm}/^\circ\text{C}$ , which is greatly improved when compared to that of conventional LPFGs (around  $+0.06 \text{ nm}/^\circ\text{C}$ ). The temperature and refractive index tuning characteristics of the LPFGs attributes to the unique material and waveguide dispersion characteristics of the proposed structure.

# ACKNOWLEDGEMENT

在交大的兩年碩士生涯中，雖然短暫但是認識很多特別的人也經歷許多事物。非常感謝我的指導教授賴暎杰老師在研究的過程中給予支持與不厭其煩地指導。賴老師雖然學富五車但是從不自滿，依然不斷學習與充實自己並對研究充滿熱忱，實在是我們的好榜樣。

感謝徐桂珠學姐、陳南光學長、李澄鈴學姊、許宜蕙學姐、項維巍學長、洪拒峰學長在研究上的指導與幫助；實驗室的好夥伴們張宏傑、辛宸瑋、鍾佩芳、池昱勳、顏子翔、張榮宏，感謝你們讓實驗室充滿歡笑；感謝我的家人對我的支持與包容；駿佑、凱婷，還有其他好朋友們，謝謝你們的陪伴，時常讓我覺得非常溫馨，有你們真好！



# CONTENTS

	<b>Page</b>
<b>Abstract (in Chinese)</b>	i
<b>Abstract (in English)</b>	ii
<b>Acknowledgement</b>	iii
<b>Contents</b>	v
<b>List of Figures</b>	vi
<b>Chapter 1 : Introduction</b>	
1.1 Fiber taper	1
1.2 Long period fiber grating	3
1.3 Motivation of the thesis	4
1.4 Structure of the thesis	5
1.5 References	6
<b>Chapter 2 : Principles</b>	
2.1 Modes in fiber taper	9
2.1-1 Mode transformation in a fiber taper	9
2.1-2 Mode solving in a step-profile three-layer fiber	11
2.2 Mode coupling through long-period grating	15
2.2-1 Coupling between two fiber modes by grating	15
2.2-2 Coupled- mode theory	21
2.3 Calculated intermodal dispersion relations	22
2.4 References	30
<b>Chapter 3 : Experiments</b>	
3.1 Fabrication of fiber tapers and long period gratings	31
3.1-1 Fabrication of fiber tapers	31
3.1-2 Fabrication of long period gratings	33
3.2 measurement setup and results	38
3.3 Environment effects and applications	45
3.4 References	49
<b>Chapter 4 : Conclusion</b>	51

# LIST OF FIGURES

Fig.1.1	Structure of a tapered fiber.....	2
Fig.1.2	Structure of Conventional photo-induced long-period fiber grating .....	4
Fig.2.1	The step-profile three-layer fiber. ....	12
Fig.2.2	Diffraction of light wave by grating.....	16
Fig.2.3(a)	LPFG resonances for two modes coupled are found by the intersection of the inter modal dispersion function $\Phi(\lambda)$ and the horizontal line represent the spatial period of the grating. When the period changes from $\Lambda$ to $\Lambda'$ , the resonant wavelength shifts from $\lambda_m$ to $\lambda_m'$ .....	18
Fig.2.3(b)	When the period changes from $\Lambda$ to $\Lambda'$ , the resonant wavelength shifts from $\lambda_m$ to shorter wavelength $\lambda_m'$ .....	18
Fig.2.3(c)	When the period increases from $\Lambda$ to $\Lambda'$ , the dual resonant wavelengths shift toward each other.....	19
Fig.2.4(a)	Positive linear-dispersion gratings: $d\lambda_m/d\Lambda > 0$ The shift of resonant wavelengths towards longer wavelengths as increasing the period of grating.....	19
Fig.2.4(b)	Negative linear-dispersion gratings: $d\lambda_m/d\Lambda < 0$ The shift of resonant wavelengths towards shorter wavelengths as increasing the period of grating.....	20
Fig. 2.4(c)	Quadratic-dispersion gratings: $d\lambda_m/d\Lambda = 0$ . As increasing the period of grating, the dual resonant wavelengths get closer, and the split dips will merge into one dip.....	20
Fig.2.5	Dispersion relation of SMF-28 surrounding by air (cladding	

diameter:125 $\mu$ m; core diameter: 8.2 $\mu$ m).....	22
Fig.2.6 Dispersion relation of the fiber taper surrounding by air (cladding diameter: 20 $\mu$ m; core diameter: 1.312 $\mu$ m ).....	23
Fig.2.7 Dispersion relation of the fiber taper surrounding by water (n=1.33) (cladding diameter: 20 $\mu$ m; core diameter: 1.312 $\mu$ m ).....	23
Fig.2.8 Dispersion relation of the fiber taper surrounding by Cargille index-matching liquids (n=1.42 at $\lambda$ =1.46 $\mu$ m) (cladding diameter: 20 $\mu$ m; core diameter: 1.312 $\mu$ m ).....	24
Fig.2.9 Intermodal dispersion of SMF-28 surrounding by air (cladding diameter:125 $\mu$ m; core diameter: 8.2 $\mu$ m).....	26
Fig.2.10 Intermodal dispersion of the fiber taper surrounding by air (cladding diameter: 20 $\mu$ m; core diameter: 1.312 $\mu$ m in taper waist ).....	27
Fig.2.11 Intermodal dispersion of the fiber taper surrounding by water (n=1.33) (cladding diameter: 20 $\mu$ m; core diameter: 1.312 $\mu$ m in taper waist ).....	28
Fig.2.12 Intermodal dispersion relation of the fiber taper surrounding by Cargille index-matching liquids (n=1.42 at $\lambda$ =1.46 $\mu$ m) (cladding diameter: 20 $\mu$ m; core diameter: 1.312 $\mu$ m in taper waist ).....	29
Fig.2.13 Intermodal dispersion of modes M <sub>11</sub> and M <sub>01</sub> of the SMF-28 surrounded by air and the fiber taper with different surrounding media.(cladding diameter: 20 $\mu$ m; core diameter: 1.312 $\mu$ m in taper waist ).....	30

Fig. 3.1 Schematic diagram of the tapering station used to fabricate the tapered fibers. The arrows indicate the direction of movement.	
Lo is the length of oscillation of the flame torch.....	32
Fig. 3.2 Process flow of fabrication of SU-8 structure.....	34
Fig.3.3 Expose SU-8 to UV-lights through amplitude mask.....	36
Fig.3.4 The fabricated long period grating by SU-8 with the grating period is 211 $\mu\text{m}$ .....	37
Fig.3.5 Diagram of measurement setup and the long period fiber grating composed of a fiber taper and a side-contact metal grating.....	38
Fig.3.6(a)Transmission spectra of the LPFG with diameter of taper waist being 20 $\mu\text{m}$ , grating period being 421 $\mu\text{m}$ , and the surrounding medium being air (black line) or water (red line)..	40
Fig.3.6(b) Transmission spectra of the LPFG with diameter of taper waist being 20 $\mu\text{m}$ , grating period being 430 $\mu\text{m}$ , and the surrounding medium being air (black line) or water (red line)....	41
Fig.3.6(c) Transmission spectra of the LPFG with diameter of taper waist being 20 $\mu\text{m}$ , grating period being 500 $\mu\text{m}$ , and the surrounding medium being air (black line) or water (red line)....	42
Fig.3.6(d)Transmission spectra of the LPFGs. The diameter of taper waist is 20 $\mu\text{m}$ , grating period is 430 $\mu\text{m}$ (black line), 421 $\mu\text{m}$ (black line), and the surrounding medium is air. ....	44
Fig. 3.7 Transmission spectra of the LPFGs with D = 20 $\mu\text{m}$ , grating	



period = 436  $\mu\text{m}$ , and the surrounding medium is air (black line), water (blue line) and alcohol (red line)..... 46

Fig. 3.8 Transmission spectra of the LPFGs in the air at different temperatures with  $D = 20\mu\text{m}$ , grating period = 204  $\mu\text{m}$ ..... 48

Fig. 3.9 Transmission spectra of the LPFGs with  $D = 20\mu\text{m}$ , grating period = 204  $\mu\text{m}$ , and the surrounding medium is the heated Cargille index-matching liquids with the index  $n_D = 1.43$  at room temperature. .... 49



# Chapter 1.

## Introduction

### 1.1 Fiber taper

With the extensive use of optical fibers in telecommunication systems, optical fiber devices have been widely invented and applied. In-line optical fiber components are receiving more attention due to their intrinsic compatibility with fiber links. One such example is the tapered fiber device. A fiber taper is usually made by stretching a heated fiber, forming a structure comprising a narrow stretched filament (the “taper waist”). The conical section between taper waist and untapered fiber is the taper transition, as shown in Fig.1.1. The fundamental mode of the untapered fiber is transferred to cladding modes of the taper waist during the taper transition section.

With decreasing taper diameter, the evanescent tail of the guided mode spreads out across the silica–air interface, and the buried waveguide of the untapered fiber is converted to an open waveguide. Although open waveguides can also be created by fiber side polishing [1-1] or D-shaped fibers [1-2], fiber tapering technique provides an ideal solution with low excess loss [1-3]. The conservation of cylindrical symmetry also retains the mode structure of the untapered fiber.

Fiber tapering techniques have been widely used in many optical fiber devices such as

modal interferometers [1-4] and spectral filters [1-5] or sensors [1-6]. In a tapered fiber, the gradual reduction of the core and cladding diameters makes the evanescent tail of the guiding mode spread out into the cladding and reach the external environment. Based on it, many of these tapered fiber devices are based on the principle of acting directly on the guided field by the intermediary of the refractive index of the exterior with chemicals as external media. On the basis of fiber tapers, we fabricated long-period fiber gratings by using a tapered fiber side-contacted with a metal grating at the taper waist to couple the modes evanescently through the side-contact long-period grating.

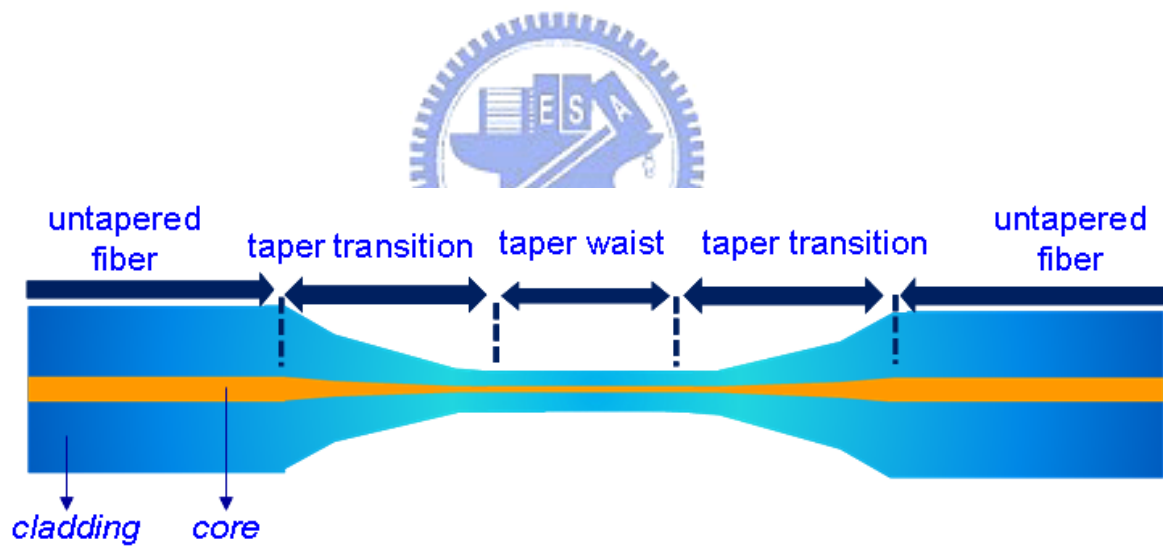
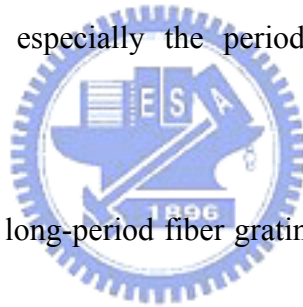


Fig. 1.1 Structure of a tapered fiber.

## 1.2 Long period fiber grating

Long-period fiber gratings (LPFG's) have been widely applied as filters [1-7] for fiber-optic telecommunications and as sensors for strain [1-8], temperature [1-9], and refractive-index [1-10] measurements. Advantages of fiber gratings include all-fiber geometry, low insertion loss, high return loss, and low cost. But the most distinguishing property of fiber gratings is the flexibility for obtaining desired spectral characteristics. There are many physical parameters can be designed including: index change, length of grating, apodization, period chirp, fringe tilt, and especially the period of grating for coupling at desired wavelengths.



Conventional photo-induced long-period fiber gratings depicted in Fig.1.2 can be made by exposing a fiber by ultra-violet (UV) lights through amplitude mask to produce the structure with the periodically varying index of the core along the fiber. The fiber used is a photosensitive fiber in, which the refractive index of the doped core can be raised by the exposure of UV lights. The magnitude of the refractive index change is typically between  $10^{-6}$  to  $10^{-3}$ , depending on the exposure time and dopants (such as Germania) concentration. The periodic index modulation for fabricating long-period fiber grating may be obtained by ion implantation [1-11], irradiation by femtosecond pulses [1-12], irradiation by CO<sub>2</sub> lasers [1-13], mechanical stress [1-14] and electrical discharges [1-15]. Another way to fabricate the

periodic structure of fibers is through periodic deformation. This is has been achieved by tapering the fiber [1-16] or by deformation of the core or cladding [1-17]. In the thesis, we fabricate long-period fiber gratings by using an external periodic structure to contact the waist of the tapered fiber. This device provides a convenient way to vary the characteristics of periodic structure for obtaining the desired transmission spectra.

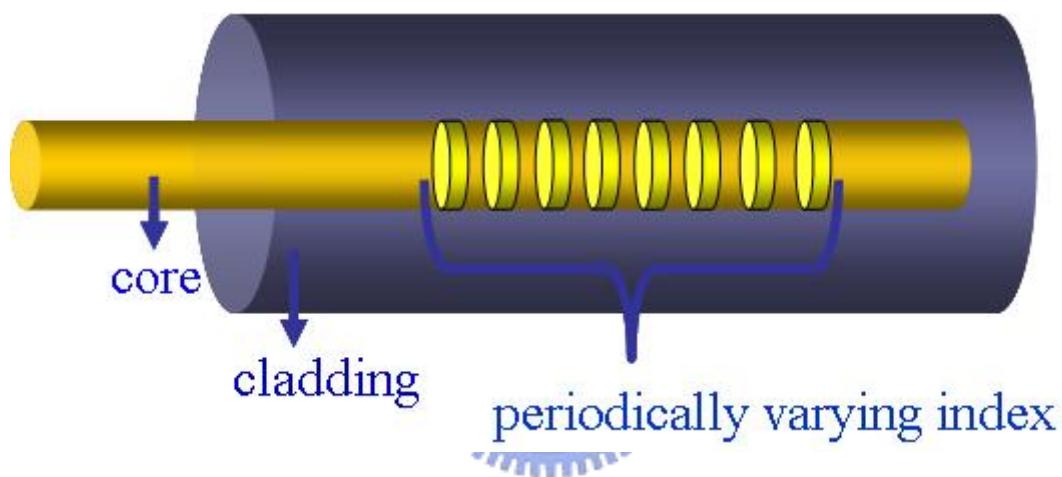


Fig. 1.2 Structure of Conventional photo-induced long-period fiber grating

### 1.3 Motivation of the thesis

Long-period fiber gratings with artificial waveguiding structures or material constituents may possess more wavelength tunability in sensing applications and may have more functionalities than conventional LPFGs. Conventional LPFGs are made by introducing

periodic index changes in the fiber core to couple the core mode with cladding modes at discrete wavelengths. In sensing applications, the conventional LPFGs have limited temperature and refractive index tuning ability due to the tight mode field confinement. Numerous kinds of LPFGs were proposed to enhance the sensitivity, such as short-grating period, ultra-thin cladding layer, CO<sub>2</sub> laser ablation, and surface-corrugated fibers. In these cases, the fiber constituents with high thermo-optic coefficients and strong overlap among the core mode, cladding modes, and the external medium, are crucial to the tuning efficiency of the LPFG dip wavelengths [1-17]-[1-20]. The slimmed-down fiber with cylindrically-symmetric surface-corrugated LPFGs had been proposed [1-21]. The strong interaction of the optical evanescent field with the environment causes much higher wavelength-dependent effective index change between the fundamental mode and higher order modes, which in turn affects the phase-matching wavelengths and mode-coupling characteristics. The field overlap among the fundamental mode and higher order modes is substantially improved, due to the fact that the higher-order modes extend farther into the external medium to yield a stronger overlap. The device is thus more sensitive to the index variation of the external medium.

## **1.4 Structure of the thesis**

The present thesis comprises four chapters. Chapter 1 is an introductory chapter consisted of an introduction to tapered fibers and long-period fiber gratings and the

motivation of our research. Chapter 2 describes the principles and analysis of our research work. It contains the theory of mode propagation in fiber taper, analysis of mode properties, the behavior of two fiber modes coupled by a grating, and an introduction to the coupled mode theory. Chapter 3 describes our experimental procedures for making LPFGs, and shows the measurement results. Finally, Chapter 4 gives the conclusions.

## 1.5 References

- [1-1] R. A. Bergh, G. Kotler, and H. J. Shaw, "Single-mode fiber optic directional coupler," *Electron. Lett.*, vol. 16, pp. 260, 1980.
- [1-2] R. B. Dyott and P. F. Schrank, "Self-locating elliptically cored fibre with an accessible guiding region" *Electron. Lett.*, Vol. 18, pp. 980-981, 1982.
- [1-3] J. D. Love and W. M. Henry, "Quantifying loss minimisation in single-mode fibre tapers" *Electronics Lett.*, Vol. 22, pp. 912-914, 1986.
- [1-4] J. Villatoro, V. P. Minkovich, and D. Monzón-Hernández, "Compact modal interferometer built with tapered microstructured optical fiber," *IEEE Photon. Technol. Lett.* 18, 1258-1260, 2006.
- [1-5] R. Feced, C. Alegria, M. N. Zervas, and R. I. Laming, "Acoustooptic attenuation filters based on tapered optical fibers," *IEEE J. Select. Top. Quantum Electron.*, vol. 5, no. 3, pp. 1278-1288, 1999.
- [1-6] J. F. Ding, A. P. Zhang, L. Y. Shao, J. H. Yan, and S. He, "Fiber-taper seeded long-period grating pair as a highly sensitive refractive-index sensor," *IEEE Photonics Technol. Lett.* 17, pp.1247-1249, 2005.
- [1-7] A. M. Vengsarkar, P. J. Lemaire, J. B. Judkins, V. Bhatia, T. Erdogan, and J. E. Sipe,

“Long-period fiber gratings as band-rejection filters,” J. Lightwave Technol., vol.14, pp.58-65, 1996.

[1-8] Liu. Y, Zhang L., and Bennion I. “Fibre optic load sensors with high transverse strain sensitivity based on long-period gratings in B/Ge co-doped fibre,” Electronics Lett., Vol. 35, pp. 661-663, 1999.

[1-9] Xuewen Shu Allsop, T. Gwandu, B. Lin Zhang Bennion, I. ,” High-temperature sensitivity of long-period gratings in B-Ge codoped fiber,” Photonics Technology Letters, IEEE, Vol. 13, pp. 818-820, 2001.

[1-10] Patrick, H.J. Kersey, A.D. Bucholtz, F. “Analysis of the response of long period fiber gratings to external index of refraction,” Lightwave Technology, vol.16, pp.1606-1612, 1998.

[1-11] Makoto Fujimaki, Yoshimichi Ohki, John L. Brebner, and Sjoerd Roorda, “Fabrication of long-period optical fiber gratings by use of ion implantation,” Optics Letters, Vol. 25, Issue 2, pp. 88-89, 2000.

[1-12] Yuki Kondo, Kentaro Nouchi, Tsuneo Mitsuyu, Masaru Watanabe, Peter G. Kazansky, and Kazuyuki Hirao, “Fabrication of long-period fiber gratings by focused irradiation of infrared femtosecond laser pulses,” Optics Letters, Vol. 24, Issue 10, pp. 646-648, 1999.

[1-13] Hyung Suk Ryu, Yongwoo Park, Seong Tae Oh, Youngjoo Chung, and Dug Young Kim, ”Effect of asymmetric stress relaxation on the polarization-dependent transmission characteristics of a CO<sub>2</sub> laser-written long- period fiber grating,” Optics Letters, Vol. 28, Issue 3, pp. 155-157, 2003.

[1-14] S. Savin, M.J. F. Digonnet, G. S. Kino, and H. J. Shaw, “Tunable mechanically induced long-period fiber gratings,” Optics Letters, Vol. 25, Issue 10, pp.710-712, 2000.

[1-15] Godbout, N. Daxhelet, X. Maurier, A. Lacroix, S., ”Long-period fiber grating by electrical discharge,” Optical Communication, vol.1, pp.397-398, 1998.



- [1-16] L. Shao, J. Zhao, X. Dong, H. Y. Tam, C. Lu, and S. He, "Long-period grating fabricated by periodically tapering standard single-mode fiber," *Appl. Opt.* 47, 1549-1552, 2008.
- [1-17] N. K. Chen, D.-Y. Hsu, and S. Chi, "Widely tunable asymmetric long-period fiber grating with high sensitivity using optical polymer on laser-ablated cladding," *Opt. Lett.* vol. 32, no. 15, pp. 2082-2084, 2007.
- [1-18] S. W James and R. P Tatam, "Optical fibre long-period grating sensors: characteristics and application," *Meas. Sci. Technol.* vol. 14, pp. R49-R61, 2003.
- [1-19] J. A. Besley, T. Wang, and L. Reekie, "Fiber cladding mode sensitivity characterization for long-period gratings," *J. Lightwave Technol.* vol. 21, no. 3, pp. 848-853, 2003.
- [1-20] T. Zhu, Y. J. Rao, J. L. Wang and Y. Song, "A highly sensitive fiber-optic refractive index sensor based on an edge-written long-period fiber grating," *IEEE Photon. Technol. Lett.* vol. 19, no. 24, pp. 1946-1948, 2007.
- [1-21] W. Ding, and S. R. Andrews, "Modal coupling in surface-corrugated long-period-grating fiber tapers," *Opt. Lett.* vol. 33, no. 7, pp. 717-719, 2008.

# Chapter 2

## Principles

### 2.1 Modes in fiber taper

#### 2.1-1 Mode transformation in a fiber taper

Assuming that the cladding and the core radius maintains their initial ratio during fiber tapering, the decreasing of the radius of the fiber during the taper transition will result in the decreasing of the  $V$  parameter of the fiber. It has been shown in [2-1] that when the radius of the core reduces to a value so as to make the  $V$  parameter less than 1.0, the fiber ceases to be single mode. When the  $V$  parameter goes below 1.0, light cannot be confined in the core region and will guide by the cladding-air boundary with the original cladding acting as the core and the air acting as the new cladding. The light from the fundamental core mode will be transferred to the fundamental cladding mode. This process also continues in the expanding taper transition region where the radius increases and  $V$  grows to above 1.0. In the expanding taper transition, the optical power remaining in the fundamental cladding mode will be transferred to the fundamental core mode, and the power in the higher order cladding modes stays in the cladding and will be lost eventually.

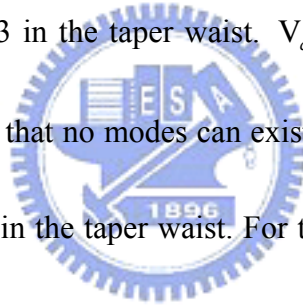
To distinguish the two cases of light guiding by the cladding-surrounding boundary and the core-cladding boundary, the corresponding  $V$  parameters will be identified respectively by

$V_{cladd}$  and  $V_{core}$  [2-2]. Here  $V_{cladd}$  and  $V_{core}$  are defined as

$$V_{core} = \frac{2\pi}{\lambda} r_{core} [n_{core}^2 - n_{cladd}^2]^{1/2} \quad (2.1)$$

$$V_{cladd} = \frac{2\pi}{\lambda} r_{cladd} [n_{cladd}^2 - n_{sur}^2]^{1/2} \quad (2.2)$$

where  $\lambda$  is the wavelength,  $r_{core}$  is the radius of the core,  $n_{core}$  and  $n_{cladd}$  are the refractive indices of the core and cladding, respectively, and  $n_{sur}$  is the refractive index of surrounding medium. The V parameter is a normalized characteristic parameter of the fiber, and it gives information about the number of modes that can propagate inside the fiber. In the case of a single mode fiber taper with a diameter of 20  $\mu\text{m}$  in the taper waist,  $V_{core}$  is about 0.36, and  $V_{cladd}$  is about 42.23 in the taper waist.  $V_{core}$  is less than 1.0 and  $V_{cladd}$  is much greater than 2.405. This means that no modes can exist in the core, and there are hundreds of modes guiding in the cladding in the taper waist. For this reason, within a fiber taper we can find a single mode–multimode transition and a multimode–single mode transition.



## 2.1-2 Mode solving in a step-profile three-layer fiber

The analysis of mode propagation in tapered fibers takes account of the refractive index profile over the whole cross-section and the taper geometry. We consider the fiber taper as a three-layer structure which composed of a core embedded in a finite cladding which is surrounded by air. The cross-section of a fiber taper is variant along the axis, therefore, there is no exact analytic solution of Maxwell's equations generally. There are several approaches to perform an analysis in such a case, but the concept of local modes [2-1] is the most intuitive and simplest. The concept of local modes is assumes that the fiber taper is slowly varying, and the modes in a fiber taper at any point along the fiber axis are equal to the modes of a straight fiber with the same core diameter. Hence the modes of such a fiber are approximations to the solutions of Maxwell's equations within local regions. Since we side-contact the waist of fiber taper with the grating, we only need to calculate the modes in the section of the uniform taper waist. Another assumption we have made is that the ratio of the diameters of cladding and core remains constant during tapering.

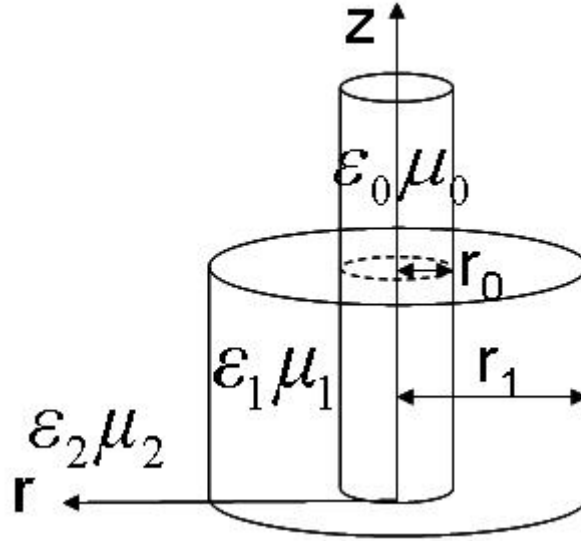


Fig.2.1 The step-profile three-layer fiber

The step-profile three-layer fiber is depicted in Fig.2.1. The  $r_0$  and  $r_1$  is the radius of core and cladding in fiber respectively. The core with constitutive parameters  $\mu_0$  and  $\epsilon_0$  embedded in the cladding with  $\mu_1$  and  $\epsilon_1$ , which is surrounded by the external medium with  $\mu_2$  and  $\epsilon_2$ . The fields and the propagation constants of the modes can be obtained by solving the appropriate boundary-value problem of the wave guiding equations, which is shown as follows.

The wave guiding equation for longitudinal components of the fields ( $E_z$  and  $H_z$ ) in the cylindrical polar coordinates  $(r, \phi, z)$  with the  $z$ -axis along the axis of the fiber is given by:

$$\left[ \frac{1}{r} \frac{\partial}{\partial r} \left( r \frac{\partial}{\partial r} \right) + \frac{1}{r} \frac{\partial^2}{\partial \phi^2} + k_r^2 \right] \begin{cases} E_z \\ H_z \end{cases} = 0, \text{ where } k_r^2 = \omega^2 \mu \epsilon - k_z^2 \quad (2.3)$$

Inside the core, solutions for  $E_z$  and  $H_z$  are Bessel functions

$$E_z = A J_m(k_{r_0} r) \cos(m\phi) e^{ik_z z} \quad (2.4a)$$

$$H_z = B J_m(k_{r_0} r) \sin(m\phi) e^{ik_z z} \quad (2.4b)$$

$$\text{with the following relation for the } k \text{ constants : } k_z^2 + k_{r_0}^2 = \omega^2 \varepsilon_0 \mu_0 \quad (2.4c)$$

In the cladding region, solutions for  $E_z$  and  $H_z$  are

$$E_z = CJ_m(k_{r_1}r)\cos(m\phi)e^{ik_z z} + DY_m(k_{r_1}r)\cos(m\phi)e^{ik_z z} \quad (2.5a)$$

$$H_z = FJ_m(k_{r_1}r)\sin(m\phi)e^{ik_z z} + GY_m(k_{r_1}r)\sin(m\phi)e^{ik_z z} \quad (2.5b)$$

$$\text{with } k_z^2 + k_{r_1}^2 = \omega^2 \varepsilon_1 \mu_1 \quad (2.5c)$$

In the surrounding, the field associated with the guiding wave is evanescent in the radial direction. Let  $k_{r_2} = i\alpha_{r_2}$ . The solutions in the surrounding are

$$E_z = IH_m^{(1)}(i\alpha_{r_2}r)\cos(m\phi)e^{ik_z z}, \quad (2.6a)$$

$$H_z = JH_m^{(1)}(i\alpha_{r_2}r)\sin(m\phi)e^{ik_z z}, \quad (2.6b)$$

$$\text{with } k_z^2 + k_{r_2}^2 = \omega^2 \varepsilon_2 \mu_2 \quad (2.6c)$$

In the above solutions,  $J_m$  and  $Y_m$  are the Bessel functions of the first and second kind respectively, and  $H_m^{(1)}$  is the Hankel function. There are eight constants A, B, C, D, F, G, I, and J to be solved by boundary conditions at interfaces between different dielectric media. We obtain following four equations at  $r = r_0$ ,

$$AJ_m(k_{r_0}r_0) - CJ_m(k_{r_1}r_0) - DY_m(k_{r_1}r_0) = 0 \quad (2.7a)$$

$$BJ_m(k_{r_0}r_0) - FJ_m(k_{r_1}r_0) - GY_m(k_{r_1}r_0) = 0 \quad (2.7b)$$

$$\begin{aligned} & A \frac{\omega \varepsilon_0}{k_{r_0} r_0} J_m'(k_{r_0} r_0) + B \frac{m k_z}{k_{r_0}^2 r_0^2} J_m(k_{r_1} r_0) - C \frac{\omega \varepsilon_1}{k_{r_1} r_0} J_m'(k_{r_1} r_0) - D \frac{\omega \varepsilon_1}{k_{r_1} r_0} Y_m'(k_{r_1} r_0) \\ & - F \frac{m k_z}{k_{r_1}^2 r_0^2} J_m(k_{r_1} r_0) - G \frac{m k_z}{k_{r_1}^2 r_0^2} Y_m(k_{r_1} r_0) = 0 \end{aligned} \quad (2.7c)$$

$$A \frac{m k_z}{k_0^2 r_0^2} J_m(k_{r_0} r_0) + B \frac{\omega \mu_0}{k_{r_0} r_0} J_m'(k_{r_0} r_0) - C \frac{m k_z}{k_{r_1}^2 r_0^2} J_m(k_{r_1} r_0) - D \frac{m k_z}{k_{r_1}^2 r_0^2} Y_m(k_{r_1} r_0)$$

$$-F \frac{\omega\mu_1}{k_{r_1}r_0} J_m'(k_{r_1}r_0) - G \frac{\omega\mu_1}{k_{r_1}r_0} Y_m'(k_{r_1}r_0) = 0 \quad (2.7d)$$

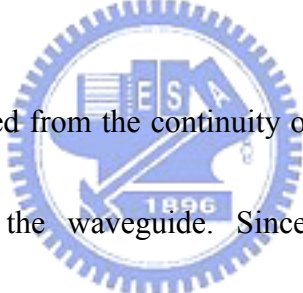
and the other for boundary conditions at  $r = r_1$ ,

$$CJ_m(k_{r_1}r_1) + DY_m(k_{r_1}r_1) - IH_m(i\alpha_{r_2}r_1) = 0 \quad (2.8a)$$

$$FJ_m(k_{r_1}r_1) + GY_m(k_{r_1}r_1) - JH_m(i\alpha_{r_2}r_1) = 0 \quad (2.8b)$$

$$\begin{aligned} C \frac{\omega\varepsilon_1}{k_{r_1}r_1} J_m'(k_{r_1}r_1) + D \frac{\omega\varepsilon_1}{k_{r_1}r_1} Y_m'(k_{r_1}r_1) + F \frac{mk_z}{k_{r_1}^2r_1^2} J_m(k_{r_1}r_1) \\ + G \frac{mk_z}{k_{r_1}^2r_1^2} Y_m(k_{r_1}r_1) + I \frac{i\omega\omega_2}{\alpha_{r_2}r_1} H'_m(i\alpha_{r_2}r_1) + J \frac{mk_z}{\alpha_{r_2}^2r_1^2} H_m(i\alpha_{r_2}r_1) = 0 \end{aligned} \quad (2.8c)$$

$$\begin{aligned} C \frac{mk_z}{k_{r_1}^2r_1^2} J_m(k_{r_1}r_1) + D \frac{mk_z}{k_{r_1}^2r_1^2} Y_m(k_{r_1}r_1) + F \frac{\omega\mu_1}{k_{r_1}^2r_1^2} J_m'(k_{r_1}r_1) \\ + G \frac{\omega\mu_1}{k_{r_1}^2r_1^2} Y_m'(k_{r_1}r_1) + I \frac{mk_z}{\alpha_{r_2}^2r_1^2} H'_m(i\alpha_{r_2}r_1) + J \frac{i\omega\omega_2}{\alpha_{r_2}r_1} H'_m(i\alpha_{r_2}r_1) = 0 \end{aligned} \quad (2.8d)$$



These eight equations resulted from the continuity of  $E_z$ ,  $H_z$  and  $E_\phi$ ,  $H_\phi$  give rise to the guidance conditions for the waveguide. Since the eight equations are a set of homogeneous linear equations, and the determinant of the coefficient matrix has to be zero in order to have non-zero solution. This condition is the final characteristic equation for determining the dispersion relation of the modes.

## 2.2 Mode coupling through long period grating

### 2.2-1 Coupling between two fiber modes by grating

The phase matching condition for a light wave incidenting on a grating at an angle  $\theta_1$  can be described by the following equation [2-3]:

$$n\sin\theta_2 = n\sin\theta_1 + m\frac{\lambda}{\Lambda}, \quad (2.9)$$

where  $\theta_2$  is the angle of the diffracted wave and the integer  $m$  determines the diffraction order (see Fig.2.2). The coupling in long period fiber gratings (a type of transmission gratings) is between the modes traveling in the same direction because the grating period is much longer than fiber Bragg gratings (FBG). We can rewrite the phase matching equation in the form:

$$\beta_2 = \beta_1 + m\frac{2\pi}{\Lambda}, \quad (2.10)$$

where  $\beta_1$  and  $\beta_2$  are propagation constants of incident wave and diffracted wave. We can consider that the grating provides an increment in propagation constant and results in coupling of two waves (modes).



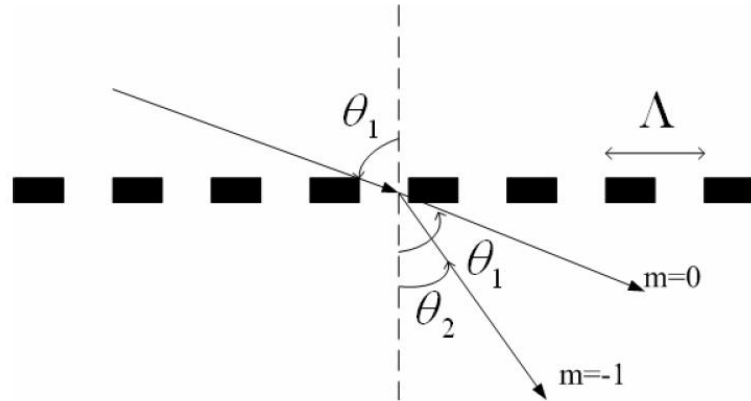


Fig.2.2 Diffraction of light wave by grating

In order to couple lights efficiently between two modes at a resonant wavelength  $\lambda_m$ , it requires that the specific period of a long-period grating  $\Lambda$  to satisfy the phase-matching condition [2-4]:

$$\Phi(\lambda) \equiv \frac{2\pi(n_{\text{eff},1} - n_{\text{eff},2})}{\lambda} = \frac{2\pi}{\Lambda}, \quad (2.11)$$

where  $n_{\text{eff},1}$  and  $n_{\text{eff},2}$  are the effective indices of the two modes.

The resonances between the modes can be determined graphically as the intersection(s) of the intermodal dispersion function with the grating spatial frequency  $2\pi/\Lambda$ . If one stretches the fiber or changes the temperature to alter the period of grating, the resonant wavelength will shift with the grating period to satisfy the phase-matching condition. Most fiber strain sensors or temperature sensors operate in this manner by measuring the change in resonant wavelength to conjecture those physical parameters. For coupling between the

modes 1 in Fig. 2.3(a), the resonant wavelength  $\lambda_m$  is increasing when the grating period  $\Lambda$  is increasing. For coupling between the modes 2 in Fig. 2.3(b), the resonant wavelength  $\lambda_m$  shifts toward shorter wavelength as the grating period  $\Lambda$  increasing. It is more complicated for the coupling between modes 3 in Fig.2.3(c). When operating near the base of the parabola, changing the grating period may alters the coupling strength but leaves the resonant wavelength fixed. When operating apart from the base of the parabola, there are two resonant wavelengths satisfying phase-matching condition, and the resonance will splits into two peaks. Dual resonance wavelengths get closer as period  $\Lambda$  increasing.

The shift of resonant wavelengths as increasing the period in the above three types of intermodal dispersion function  $\Phi(\lambda)$  are shown in Fig.2.4(a)-(c). Therefore, we can distinguish three types of long-period fiber grating: positive linear-dispersion gratings ( $d\lambda_m/d\Lambda > 0$ ), negative linear-dispersion gratings ( $d\lambda_m/d\Lambda < 0$ ), and quadratic-dispersion gratings ( $d\lambda_m/d\Lambda = 0$ ).

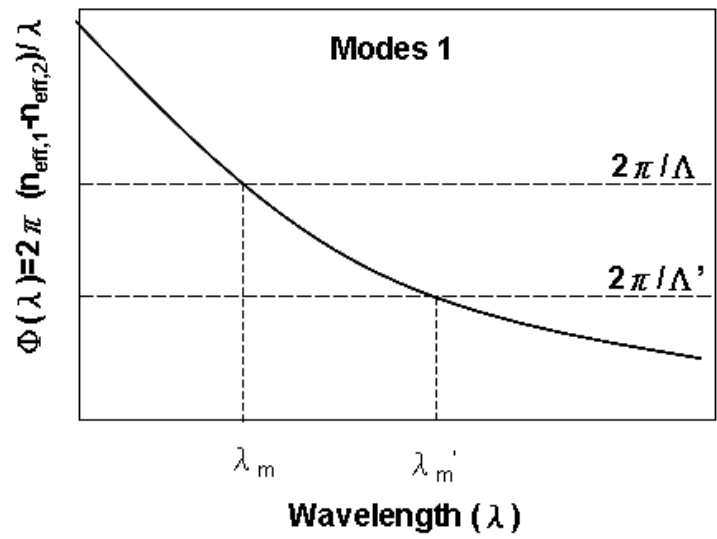


Fig.2.3(a) LPFG resonances for two modes coupled are found by the intersection of the inter modal dispersion function  $\Phi(\lambda)$  and the horizontal line represent the spatial period of the grating. When the period changes from  $\Lambda$  to  $\Lambda'$ , the resonant wavelength shifts from  $\lambda_m$  to  $\lambda'_m$ .

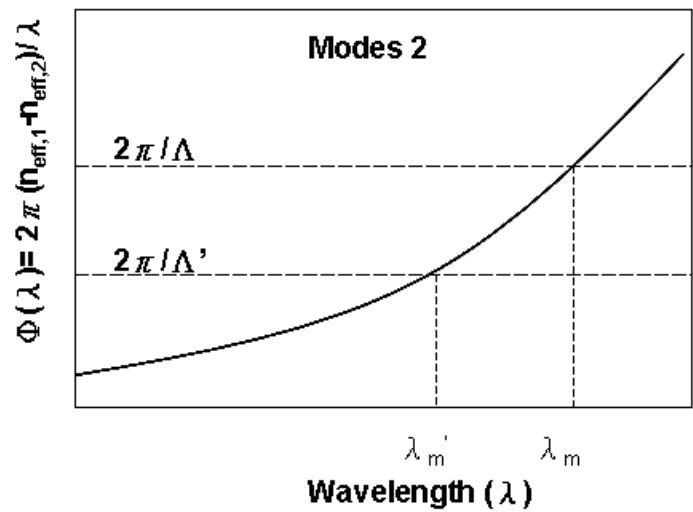


Fig.2.3(b) When the period changes from  $\Lambda$  to  $\Lambda'$ , the resonant wavelength shifts from  $\lambda_m$  to shorter wavelength  $\lambda'_m$ .

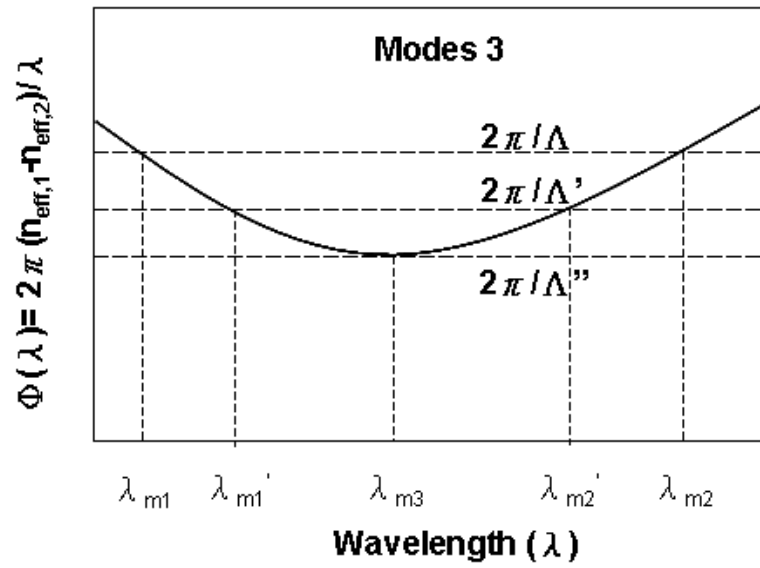


Fig.2.3(c) When the period increases from  $\Delta$  to  $\Delta'$ , the dual resonant wavelengths shift toward each other.

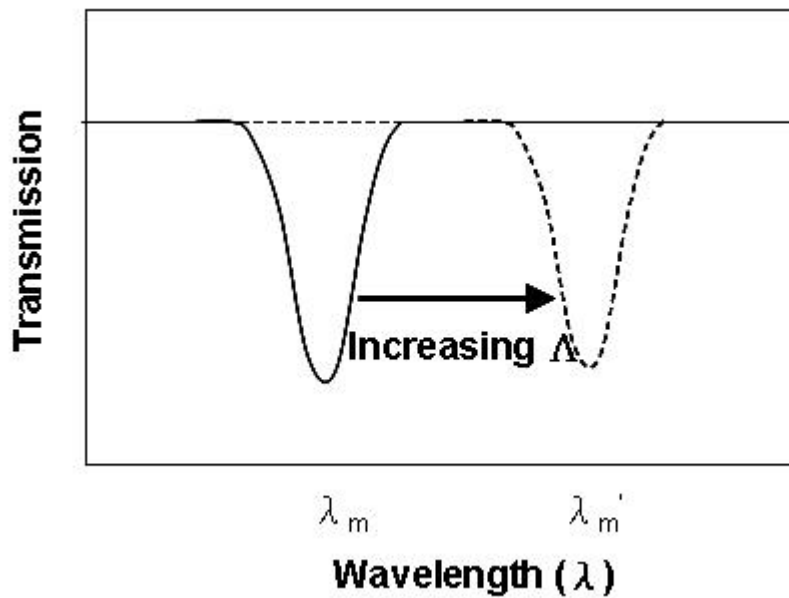


Fig.2.4( a ) Positive linear-dispersion gratings:  $d\lambda_m/d\Delta > 0$  The shift of resonant wavelengths towards longer wavelengths as increasing the period of grating.

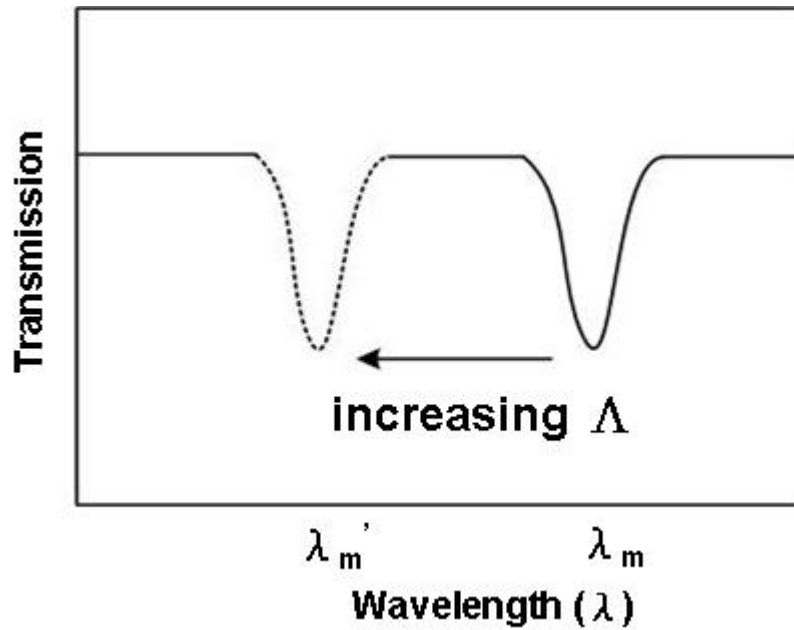


Fig.2.4( b ) Negative linear-dispersion gratings:  $d\lambda_m/d\Delta < 0$  The shift of resonant wavelengths towards shorter wavelengths as increasing the period of grating.

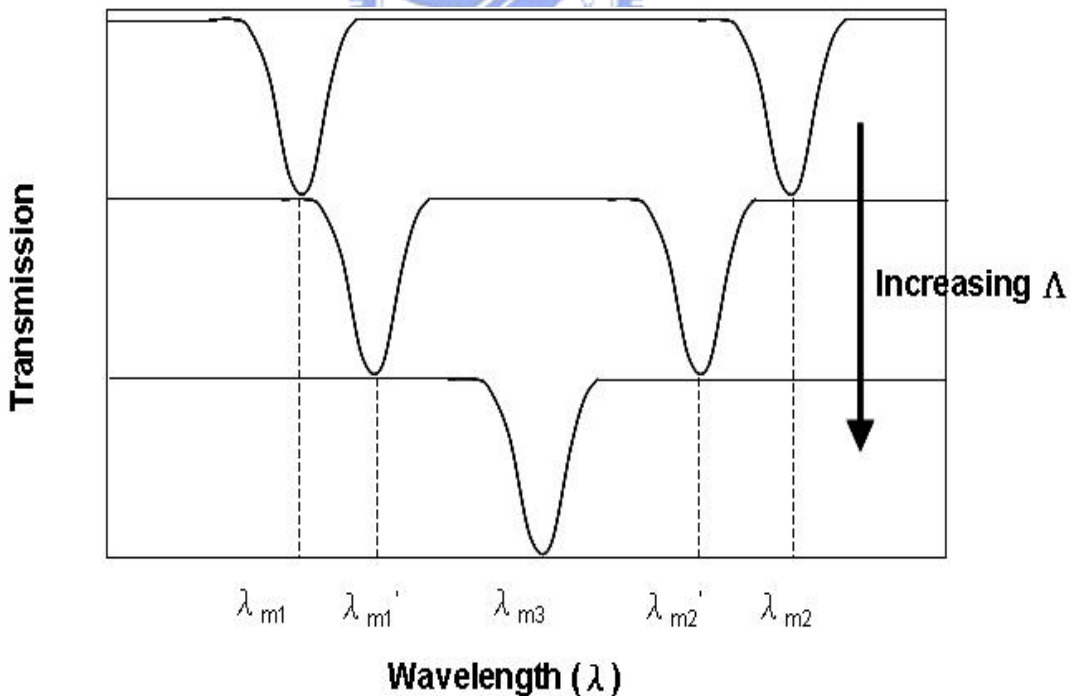


Fig. 2.4( c ) Quadratic-dispersion gratings:  $d\lambda_m/d\Delta = 0$  As increasing the period of grating, the dual resonant wavelengths get closer, and the split dips will merge into one dip.

## 2.2-2 Coupled-Mode Theory

To understand the mode propagation behavior in the long-period grating region, we apply the coupled-mode theory [2-2] to model the perturbation of a uniform waveguide and derive the field coupling terms between modes. Since the long-period fiber grating couples the forward propagating modes, the coupling equations and local coupling coefficients can be expressed as follows:

$$\frac{dA_j(z)}{dz} = \sum_1 C_{j1}(z)A_1(z) \times \exp[i(\beta_1 - \beta_j)z] , \quad (2.12)$$

$$C_{j1}(z) = \begin{cases} 0 & \text{(no grating)} \\ \int_{A_z} \frac{ik_0^2 \Delta \epsilon_r}{4\beta_j} [\hat{\mathbf{e}}_1 \times \hat{\mathbf{h}}_j^*] \cdot \hat{\mathbf{a}}_z dA & \text{(grating region)} , \end{cases} \quad (2.13)$$

where  $A_j(z)$  is the slowly varying amplitude, and  $\beta_j$  is the propagation constant of the  $j^{\text{th}}$ -order mode;  $k_0$  is the vacuum wave vector; and  $\Delta \epsilon_r$  is the change of permittivity in the grating region.  $\hat{\mathbf{e}}$  and  $\hat{\mathbf{h}}$  represent the electric and magnetic mode fields respectively;  $\hat{\mathbf{a}}_z$  is the unit vector along the fiber axis.

## 2.3 Calculated intermodal dispersion relations

We calculate the effective indices of the modes by requiring the determinant of the coefficient matrix of (2.7a-2.7d) (2.8a-2.8d) to be zero. We plot respectively the dispersion of the modes in standard single-mode fiber (SMF-28) and in the fiber tapers with the waist diameter of  $20\ \mu\text{m}$  surrounded by air, water, and Cargille index-matching liquids ( $n=1.42$  at  $\lambda=1.46\ \mu\text{m}$ ). The effective indices as a function of the wavelength for each mode are shown in the following pictures in which each mode is labeled by the notation " $M_{ml}$ ". Here the first subscript " $m$ " denotes the angular order, and the second subscript " $l$ " denotes the  $l$ th root of the characteristic equation.

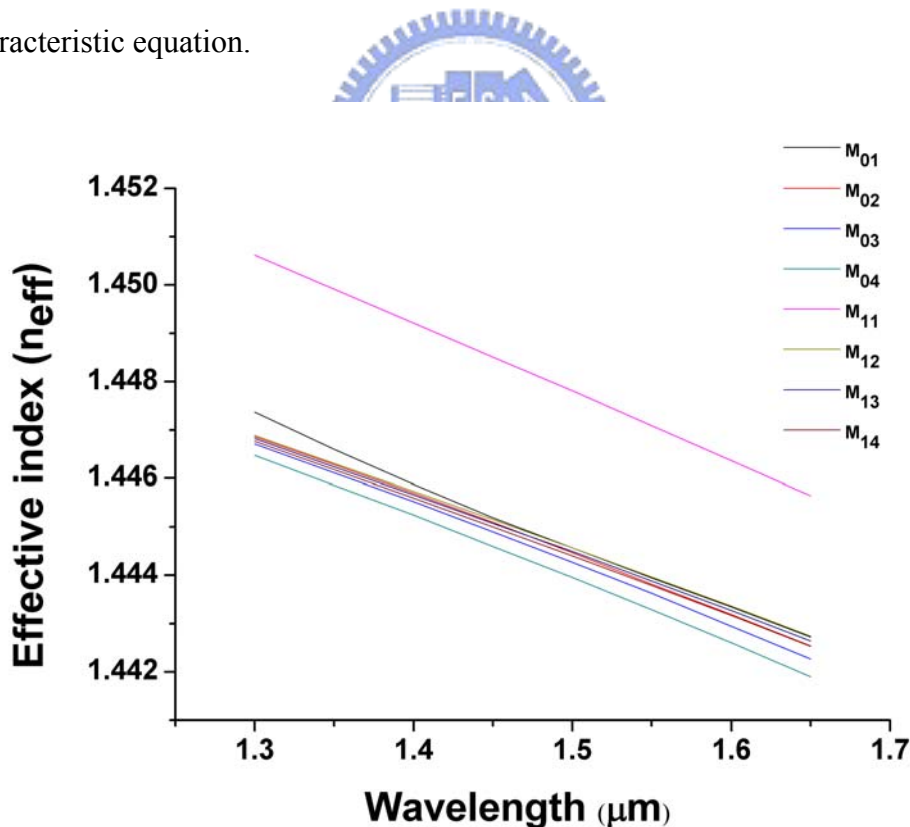


Fig.2.5 Dispersion relation of SMF-28 surrounding by air (cladding diameter:  $125\ \mu\text{m}$ ; core diameter:  $8.2\ \mu\text{m}$ )

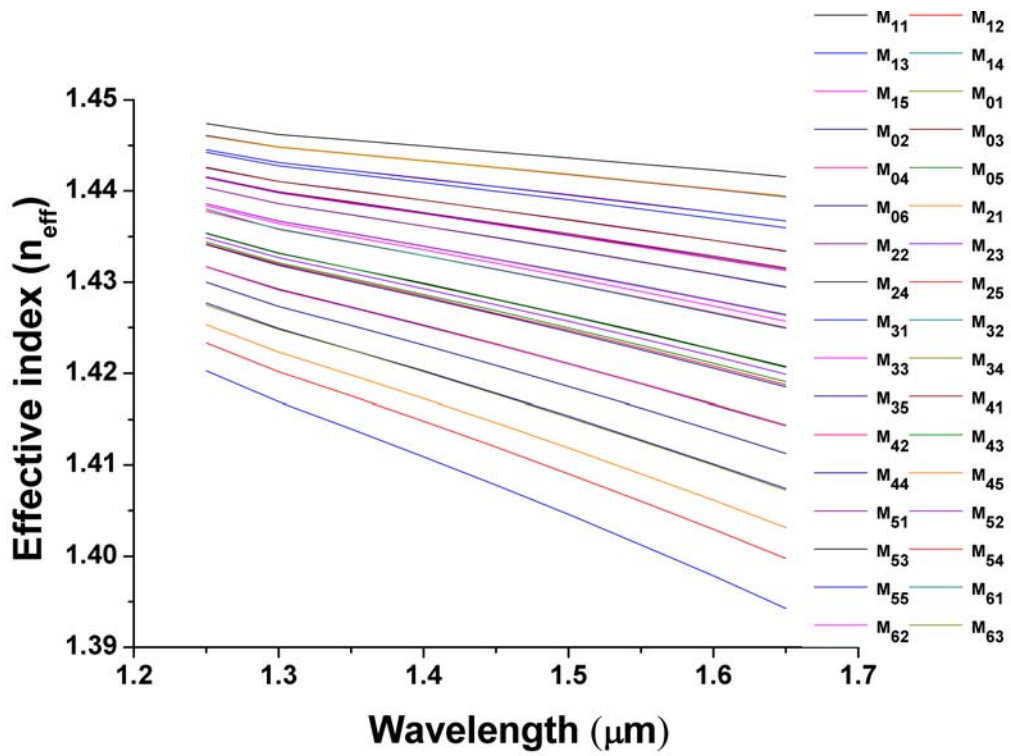


Fig.2.6 Dispersion relation of the fiber taper surrounding by air (cladding diameter:  $20 \mu m$ ; core diameter:  $1.312 \mu m$ )

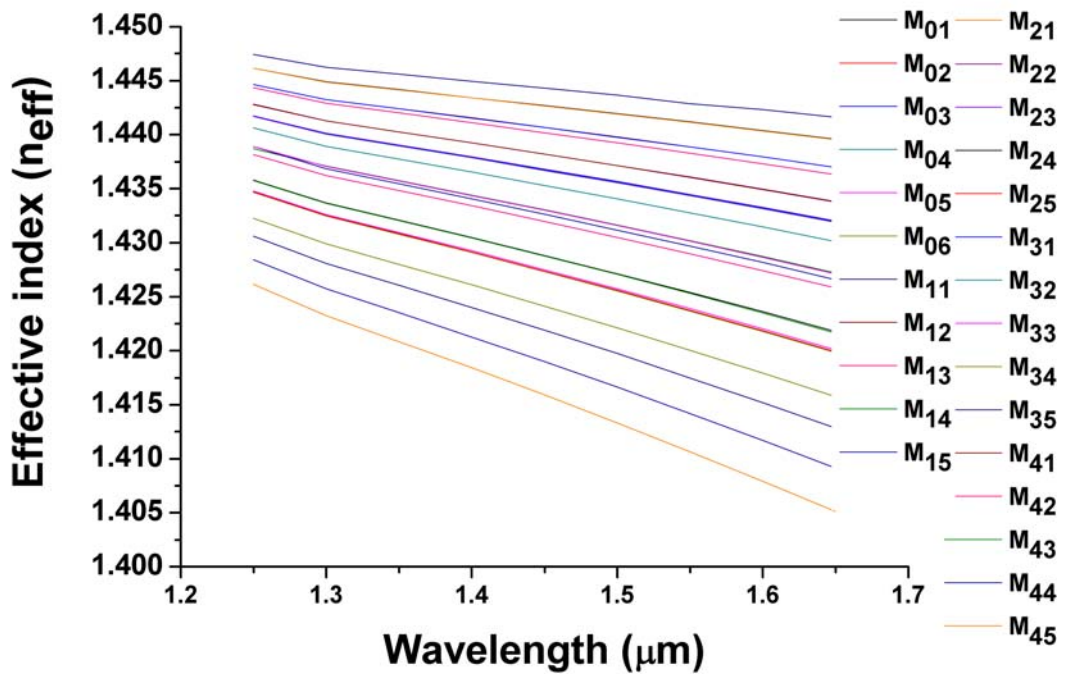


Fig.2.7 Dispersion relation of the fiber taper surrounding by water ( $n=1.33$ ) (cladding diameter:  $20 \mu m$ ; core diameter:  $1.312 \mu m$ )



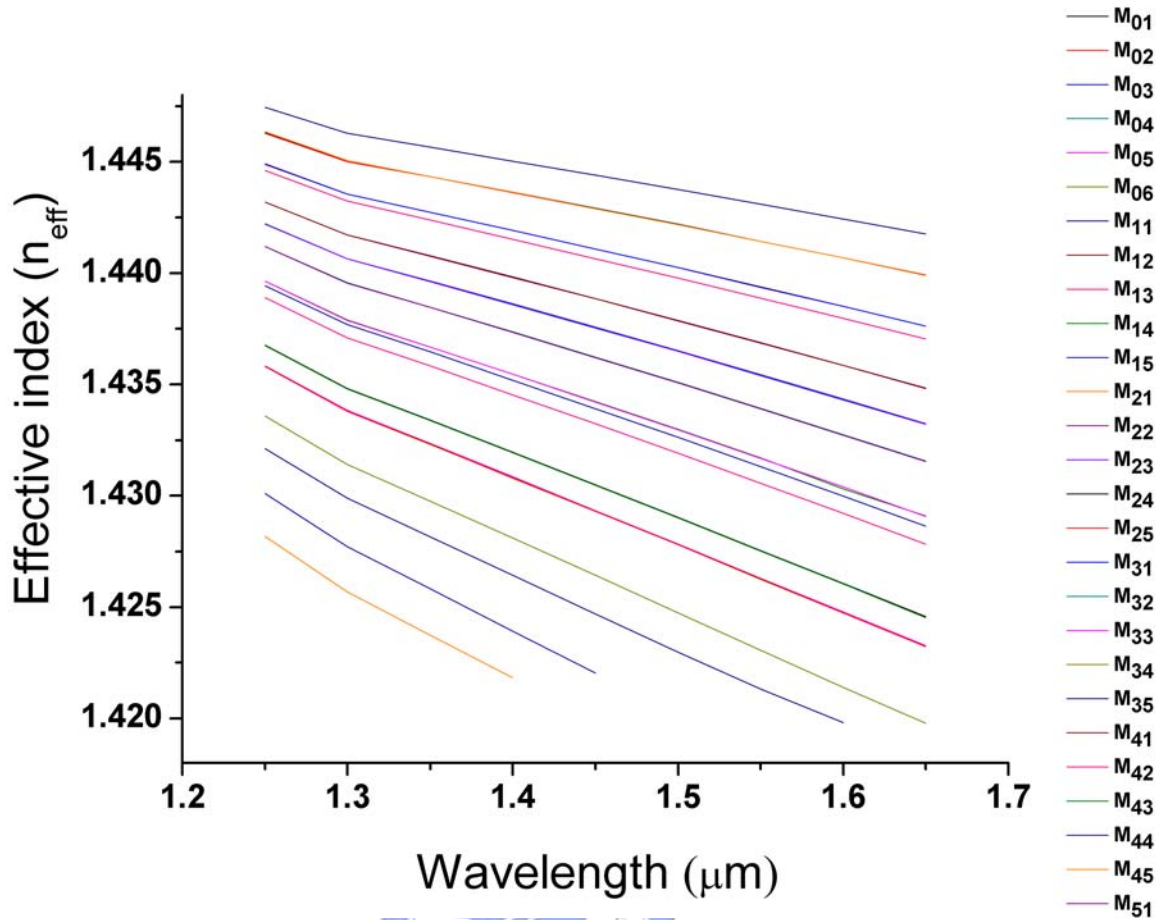


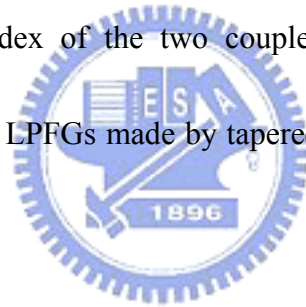
Fig.2.8 Dispersion relation of the fiber taper surrounding by Cargille index-matching liquids ( $n=1.42$  at  $\lambda=1.46\mu\text{m}$ ) (cladding diameter:  $20\ \mu\text{m}$ ; core diameter:  $1.312\ \mu\text{m}$ )

To see more clearly, we express the effective index difference in the form of the intermodal dispersion function divided by  $2\pi$ . The notation “ $M_{11-m_l}$ ” denotes that the coupling between the fundamental mode “ $M_{11}$ ” and high order mode “ $M_{m_l}$ ” are considered.

We can observe that at longer wavelengths both the core and cladding modes tends to spread out into the cladding and the surrounding medium respectively. This causes the effective index to decrease with the increasing wavelength. In a standard single-mode fiber,

the modes are confined more tightly at the cladding-air interface than at the core-cladding interface, resulting in that the effective index of the core mode decrease more progressively than that of the cladding modes. Therefore the difference of the effective index of the two coupled modes decreases with the increasing wavelength. Consequently, the conventional LPFGs made by SMF are positive linear-dispersion gratings.

In a fiber taper, the mode field of the low-order cladding modes are confined more tightly than that of the high-order modes, resulting in that the effective indices of the high-order mode decrease more progressively than those of the low-order modes. Therefore the difference of the effective index of the two coupled modes increases as the increasing wavelength. Consequently, the LPFGs made by tapered SMFs are negative linear-dispersion gratings.



In Fig.2.13 we compare the intermodal dispersion curves of  $M_{11-01}$  in a standard SMF surrounded by air and a fiber taper with three different surrounding media: air ( $n=1$ ), water ( $n=1.33$ ), and Cargille index-matching liquids ( $n=1.42$  at  $\lambda=1.46\mu\text{m}$ ). The slope of the curve is related to the grating period sensitivity. The steeper slope indicates that the phase matching wavelengths of the LPFGs are more insensitive to the grating period. The relation of the increment in the grating period and the shift in the phase matching wavelength is  $\Delta \frac{1}{\Lambda} = 0.0032\Delta\lambda_m$  in SMF-28 surrounded by air,  $\Delta \frac{1}{\Lambda} = -0.0006\Delta\lambda_m$  in the fiber taper surrounded by air,  $\Delta \frac{1}{\Lambda} = -0.000548\Delta\lambda_m$  in the fiber taper surrounded by

water,  $\Delta \frac{1}{\Lambda} = -0.000463 \Delta \lambda_m$  in the fiber taper surrounded by Cargille index-matching liquids. The sensitivity to the grating period in LPFGs made by fiber tapers becomes 5 times greater than that of the conventional LPFGs made by SMFs.

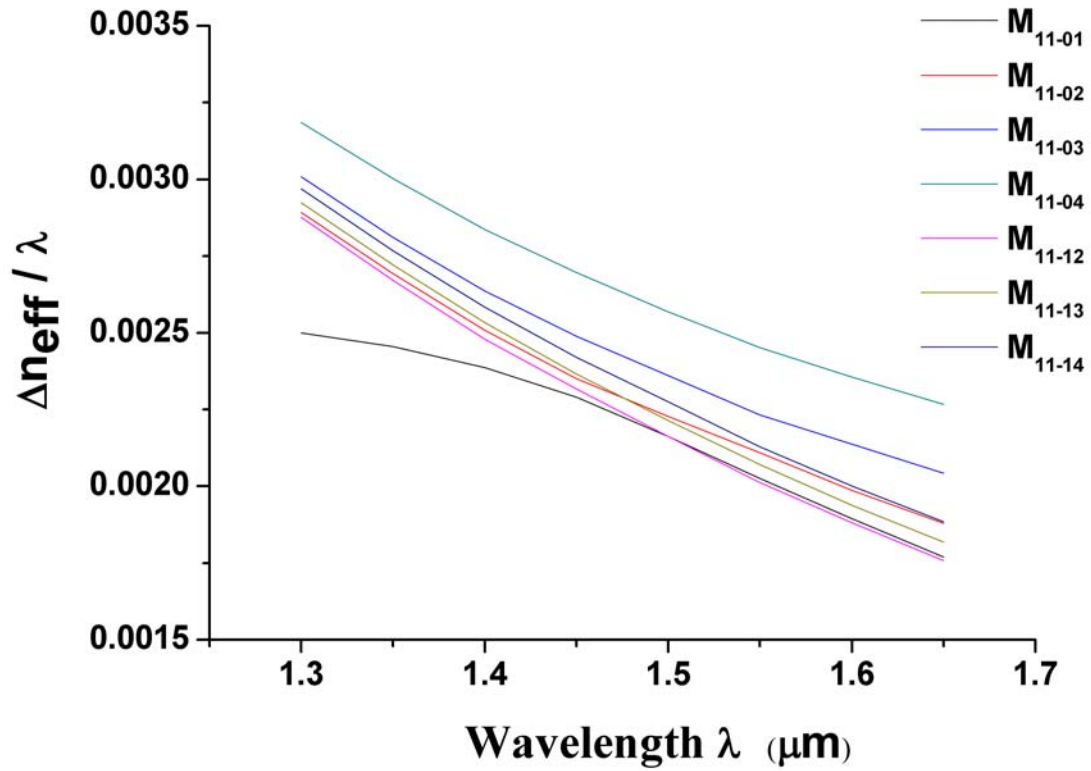


Fig.2.9 Intermodal dispersion of SMF-28 surrounding by air (cladding diameter:125 μ m; core diameter: 8.2 μ m)

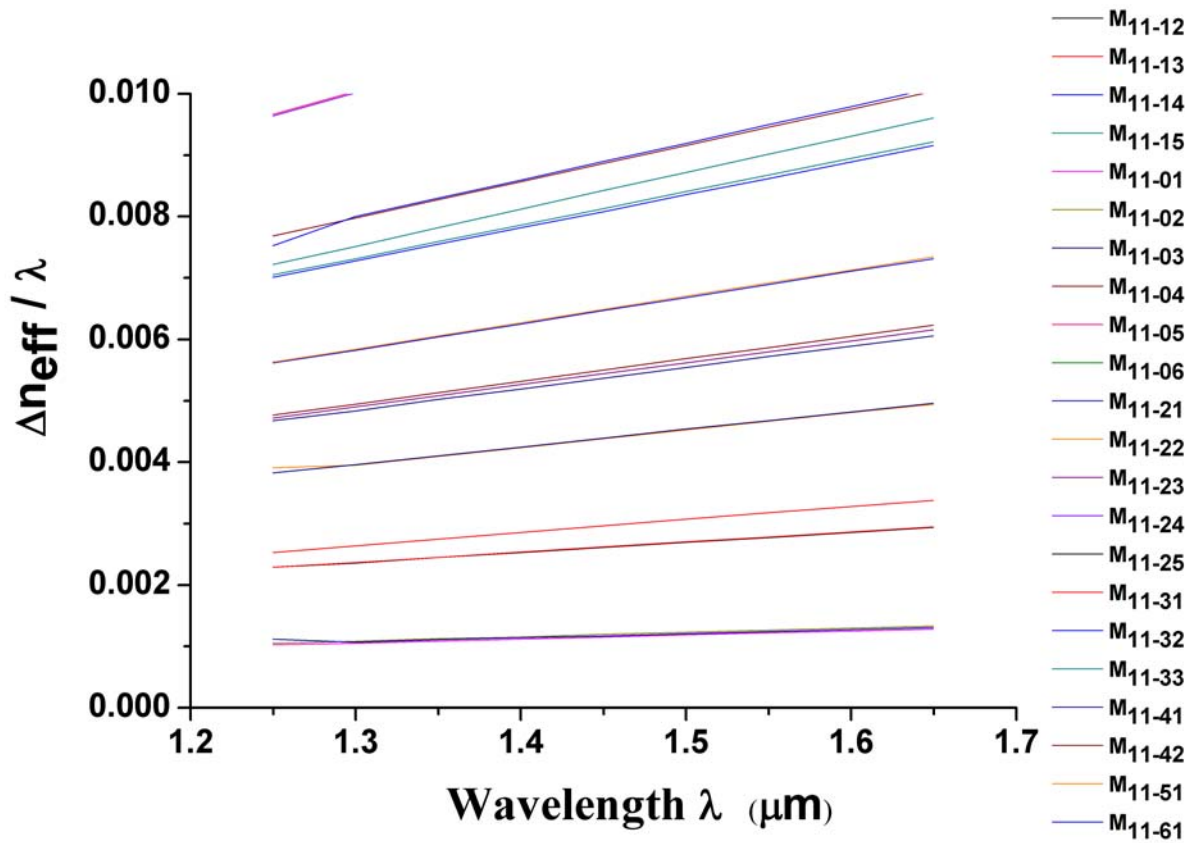


Fig.2.10 Intermodal dispersion of the fiber taper surrounding by air (cladding diameter:  $20 \mu\text{m}$ ; core diameter:  $1.312 \mu\text{m}$  in taper waist)

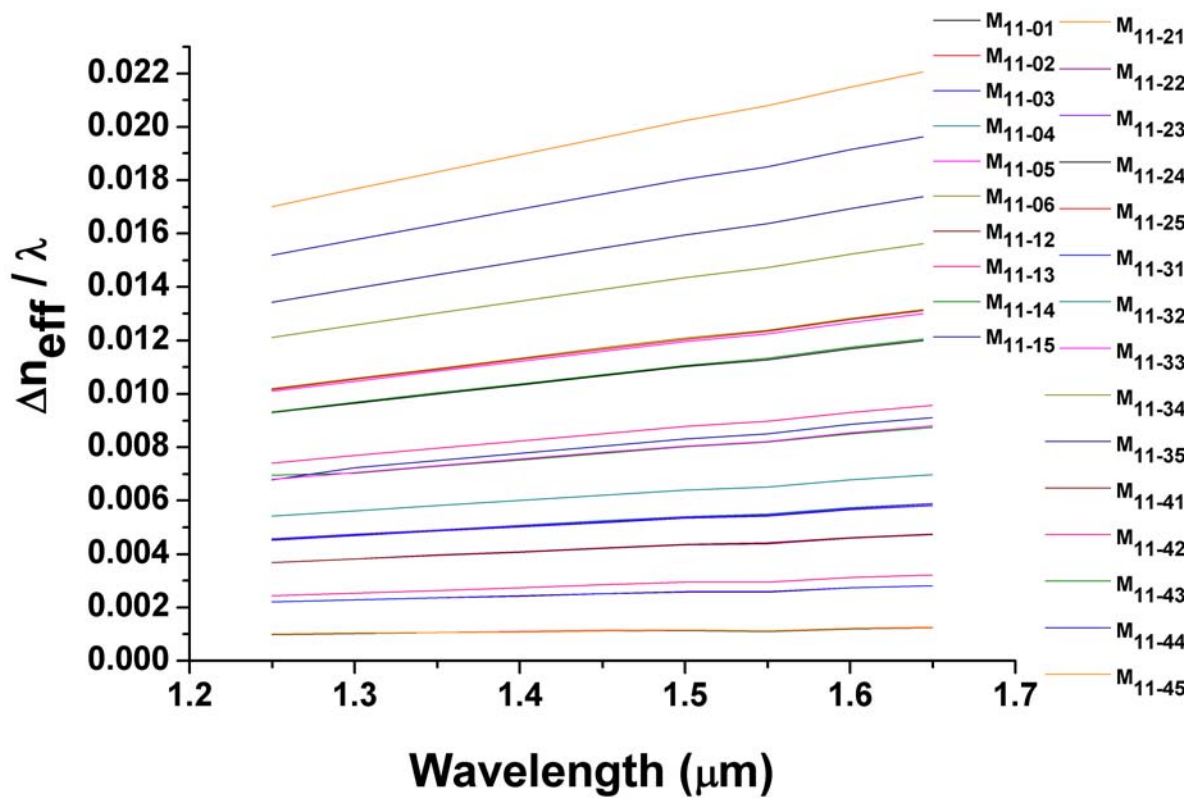


Fig.2.11 Intermodal dispersion of the fiber taper surrounding by water ( $n=1.33$ ) (cladding diameter:  $20 \mu\text{m}$ ; core diameter:  $1.312 \mu\text{m}$  in taper waist )

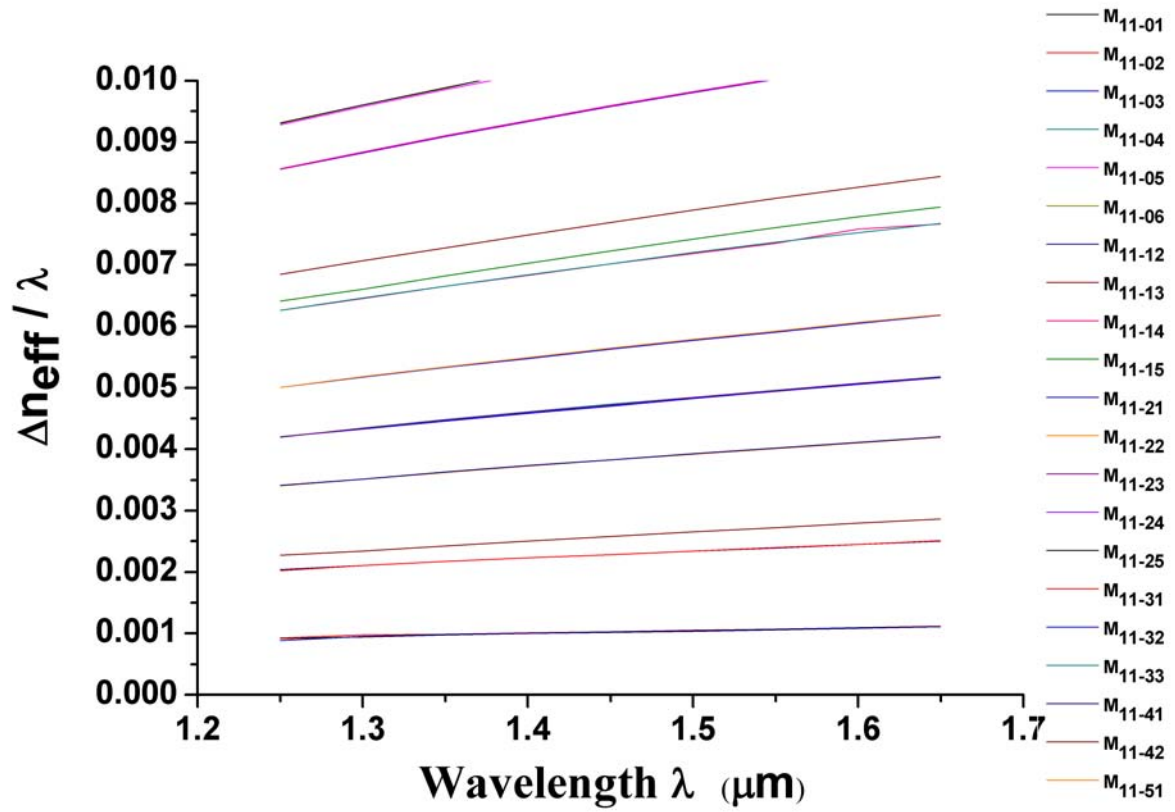


Fig.2.12 Intermodal dispersion relation of the fiber taper surrounding by Cargille index-matching liquids ( $n=1.42$  at  $\lambda = 1.46 \mu\text{m}$ ) (cladding diameter:  $20 \mu\text{m}$ ; core diameter:  $1.312 \mu\text{m}$  in taper waist )

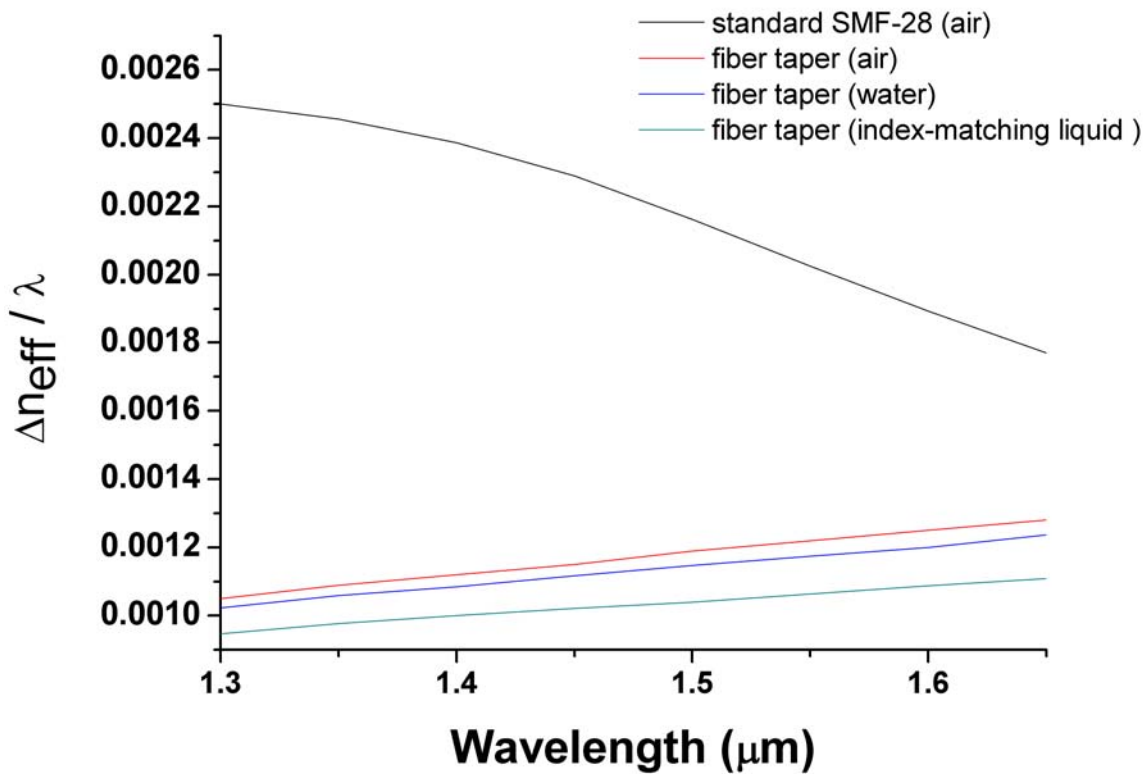


Fig.2.13 Intermodal dispersion of modes  $M_{11}$  and  $M_{01}$  of the SMF-28 surrounded by air and the fiber taper with different surrounding media.(cladding diameter:  $20 \mu\text{m}$ ; core diameter:  $1.312 \mu\text{m}$  in taper waist )

## 2.4 References

- [2-1] A. W. Snyder, J. D. Love, "Optical Waveguide Theory", Chapman and Hall, 1983.
- [2-2] Shankar, P.M. Bobb, L.C. Krumboltz, H.D. "Coupling of modes in bent biconically tapered single-mode fibers," vol. 9, pp.832-837, 1991.
- [2-3] T. Erdogan, "Fiber grating spectra," J. Lightwave Technol., vol. 15, pp.1277-1294, 1997.
- [2-4] V. Grubsky and J. Feinberg, "Long-period fiber gratings with variable coupling for real-time sensing applications," Opt. Lett. vol.25, pp.203-205, 2000.

# Chapter 3.

## Experiments

### 3.1 Fabrication of fiber tapers and long period gratings

#### 3.1-1 Fabrication of fiber tapers

The homemade tapering station (shown in Fig. 3.1) based on the “flame brush” technique [3-1] was implemented to fabricate the tapered fiber. A small flame produced by controllable hydrogen was used to heat a section of the optical fiber. The flame diameter was approximately 15 mm with a temperature of approximately 1300 °C. The flame torch was mounted on a three-axis translation stage, which in turn rested on a sliding stand driven by a stepper motor. On the one hand, the setup allows precise positioning of the flame. On the other hand, the flame is allowed to oscillate with constant speed over a distance  $L_0$ . This process ensures that the flame identically heats each section of the fiber being tapered in each cycle of oscillation. Distance  $L_0$  can be exactly controlled, therefore, the length of the uniform waist of the tapered fiber is controllable. In our experiments the speed of the flame was set to approximately 0.2 mm/s, and  $L_0$  was in the range 10-20 mm range. At the same moment when the flame starts to heat the fiber, the fiber is gently stretched in opposite directions. The pulling mechanism involves two sliding stands driven by stepper motors. The speed of the stand was approximately 0.055 mm/s. Total elongation distance  $z$  is the sum of the distances



traveled by each stand, which can also be controlled precisely. The taper station described allows the fabrication of symmetric tapers with a central region (taper waist) of constant diameter.

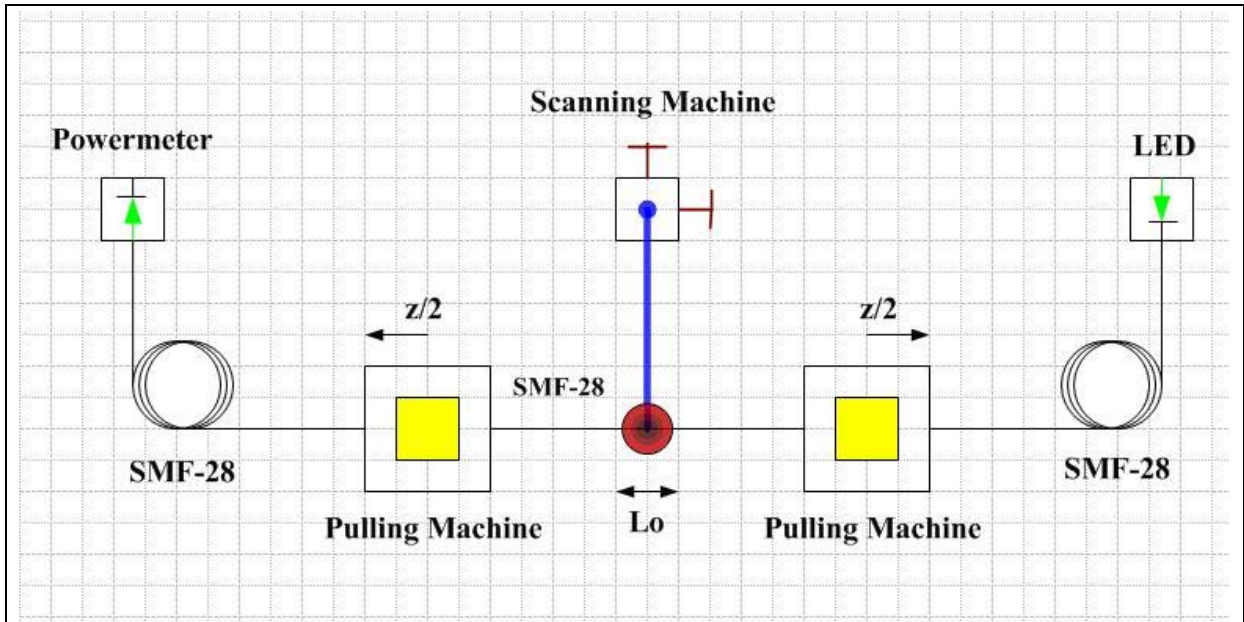


Fig. 3.1 Schematic diagram of the tapering station used to fabricate the tapered fibers. The arrows indicate the direction of movement.  $L_0$  is the length of oscillation of the flame torch.

Standard telecommunication single-mode step-index fiber (Corning SMF-28) was used to fabricate our samples in our practical tapering process. The fiber cladding-core diameters were  $125/8.2 \mu\text{m}$  with a 0.13 numerical aperture, a cutoff wavelength of 1260 nm. Before the pulling process began, the jacket was removed from the fiber over a section larger than  $L_0$ . The fiber was cleaned with ethanol. During the fabrication process the fiber must be held straight all the time. Light from a low-power LED that emits at 1410 nm

was injected into the fiber, and the output power was monitored during the whole fabrication to ensure a uniform waist. No significant fluctuations of the output signal were observed during this process. Approximately 85% of our samples had losses less than 0.5 dB. Although this value is slightly higher than the expected one, it is still negligible in a practical situation. A uniform taper waist of 20- $\mu\text{m}$  diameter is achieved by tapering down a standard single mode fiber. The length of the uniform waist is around 1 cm, and the length of the taper transition region is approximately 1.75 cm. After tapering process, in order to let the fiber taper keep straight, it was mounted on the glass-substrate by UV-adhesives at each side of untapered fiber.



### **3.1-2 Fabrication of long period gratings**

The material we used to fabricate long period gratings is SU-8 photoresist. Photoresist is a light-sensitive material widely used in microelectronic applications [3-2]. Photoresists are classified into positive resists and negative resists. A positive resist is a type of photoresist in which the portion of the photoresist that is exposed to light becomes soluble to the photoresist developer and the portion of the photoresist that is unexposed remains insoluble to the photoresist developer. A negative resist such as SU-8 is a type of photoresist in which the portion of the photoresist that is exposed to light becomes relatively insoluble to the photoresist developer. The unexposed portion of the photoresist is dissolved by the

photoresist developer. SU-8 photoresist is most commonly exposed with conventional UV (350-400 nm) radiation, although i-line (365nm) is the recommended wavelength. SU-8 may also be exposed with e-beam or x-ray radiation. Upon exposure, cross-linking proceeds in two steps: (1) formation of a strong acid during the exposure step, followed by (2) acid-catalyzed, thermally driven epoxy cross-linking during the post exposure bake (PEB) step. A normal process is: spin coat, soft bake, expose, PEB, followed by develop. A controlled hard bake is recommended to further cross-link the imaged SU-8 structures when they will remain as part of the device. The process flow is shown in Fig.3.2 Following is the detailed description of each step:

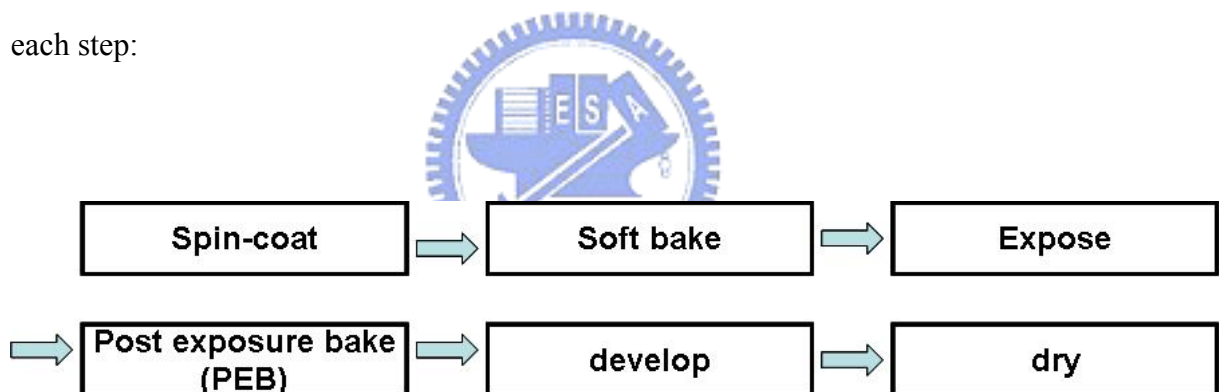


Fig. 3.2 Process flow of fabrication of SU-8 structure

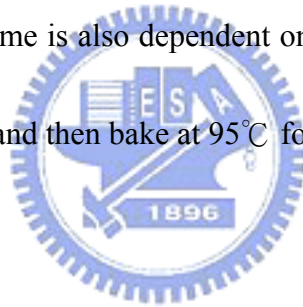
### 1. Spin coat

We use silicon wafers as substrates. To obtain maximum process reliability, substrates should be clean and dry prior to applying SU-8 resist. For best results, substrates should be cleaned with a piranha wet etch (using  $\text{H}_2\text{SO}_4$  and  $\text{H}_2\text{O}_2$ ) followed by a de-ionized water rinse. Then put the substrate in the spin coater and dispense appropriate dosage of resist in the

center of substrate. Spin at 500 rpm for 10 seconds and continuously spin at 4000 rpm for 30 seconds. Spin conditions selected depend on the desired thickness and the viscosity of SU-8. We obtain approximately uniform films of SU-8 with thickness  $25\mu\text{m}$  under the spin conditions.

## 2. Soft bake

This step is important for removing all the solvent in the film. It is in order to improve the adhesion of SU-8 with substrates and reduce stresses resulting cracks in the film. A level hotplate with good thermal control and uniformity is recommended during the soft bake step of the process. The soft bake time is also dependent on the thickness. For thickness of  $25\mu\text{m}$ , we bake at  $65^\circ\text{C}$  for 3 minutes and then bake at  $95^\circ\text{C}$  for 6 minutes.



## 3. Expose

After soft bake process, we exposed films of SU-8 by UV-lights through an amplitude mask with different grating patterns on it for 30 minutes (see Fig.3.3). The required exposure energy is depend on the thickness and desired patterns.

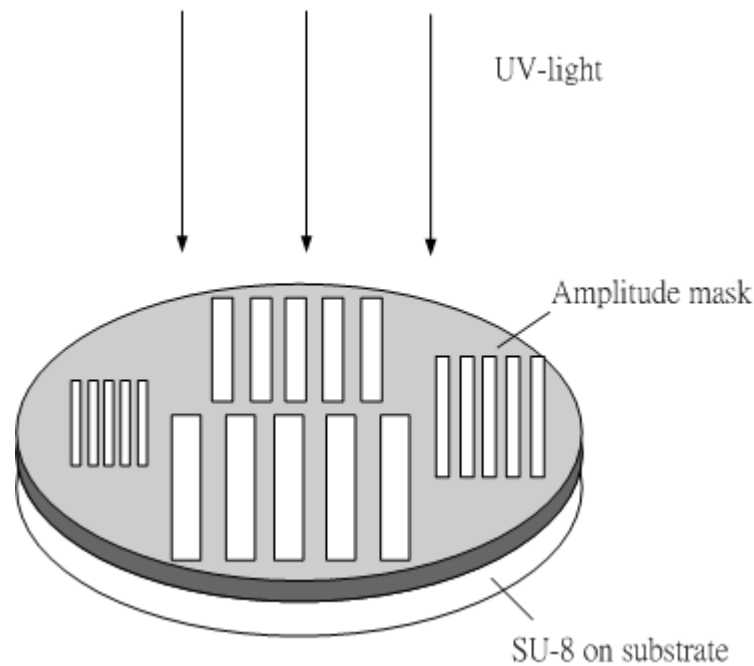
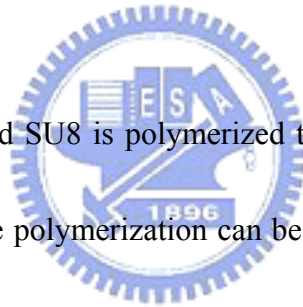


Fig.3.3 Expose SU-8 to UV-lights through amplitude mask.

#### 4. Post exposure bake

During this step the illuminated SU8 is polymerized through a chemical amplification (CA) mechanism [3-3]. Although the polymerization can be done at room temperature, we bake at 65°C for 1 minutes and then bake at 95°C for 6 minutes in order to increase the process-speed.



#### 5. Develop

SU-8 2000 photoresist has been designed for use in immersion, spray or spray-puddle processes with MicroChem's SU-8 developer. Other solvent based developers such as ethyl lactate and diacetone alcohol may also be used. Strong agitation is recommended when developing high aspect ratio or thick film structures.

#### 6. Dry

After using SU-8 developer, wash the developed image with de-ionized water, and air dry with pressed nitrogen.

The picture of the fabricated long period grating by SU-8 is shown in Fig. 3.4. The refractive index of SU-8 is approximately 1.56 at 1550nm which is higher than the index of cladding in fiber, and it will result in energy loss. Therefore, we coated a layer of stannum on gratings to reduce loss through gratings.

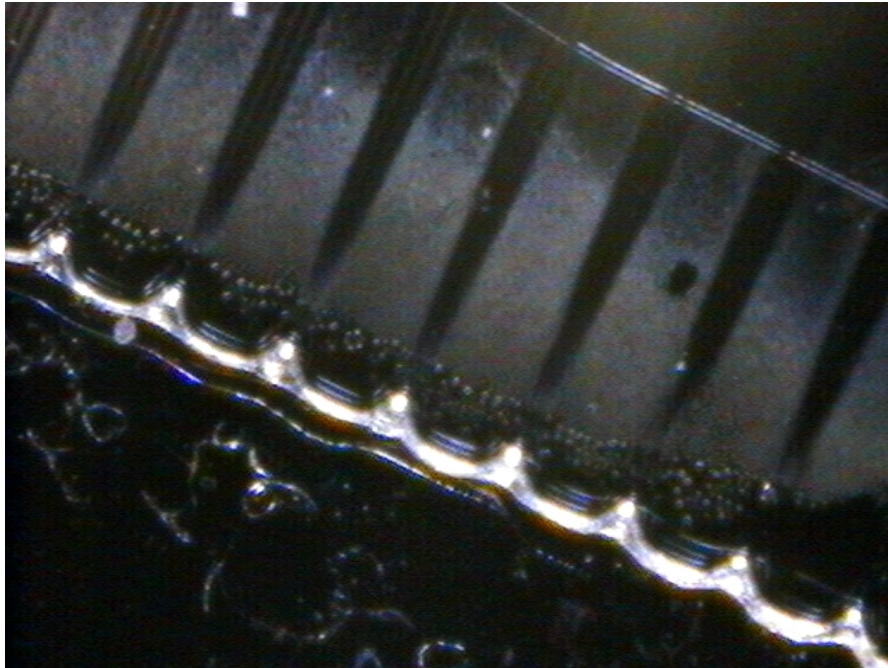


Fig. 3.4. The fabricated long period grating by SU-8 with the grating period is 211 $\mu$ m.

## 3.2 Measurement setup and results

The LPFG structure based on a fiber taper with a side-contacted metal grating and the measurement setup are shown in Fig. 3.5. A uniform taper waist of 20- $\mu\text{m}$  diameter is achieved by tapering down a standard single mode fiber (Corning SMF-28). The length of the uniform waist is around 1 cm, and the length of the taper transition region is approximately 1.75 cm. A one-dimensional thin-stannum-layer grating of total length about 1 cm is side-contacted with the taper fiber waist.

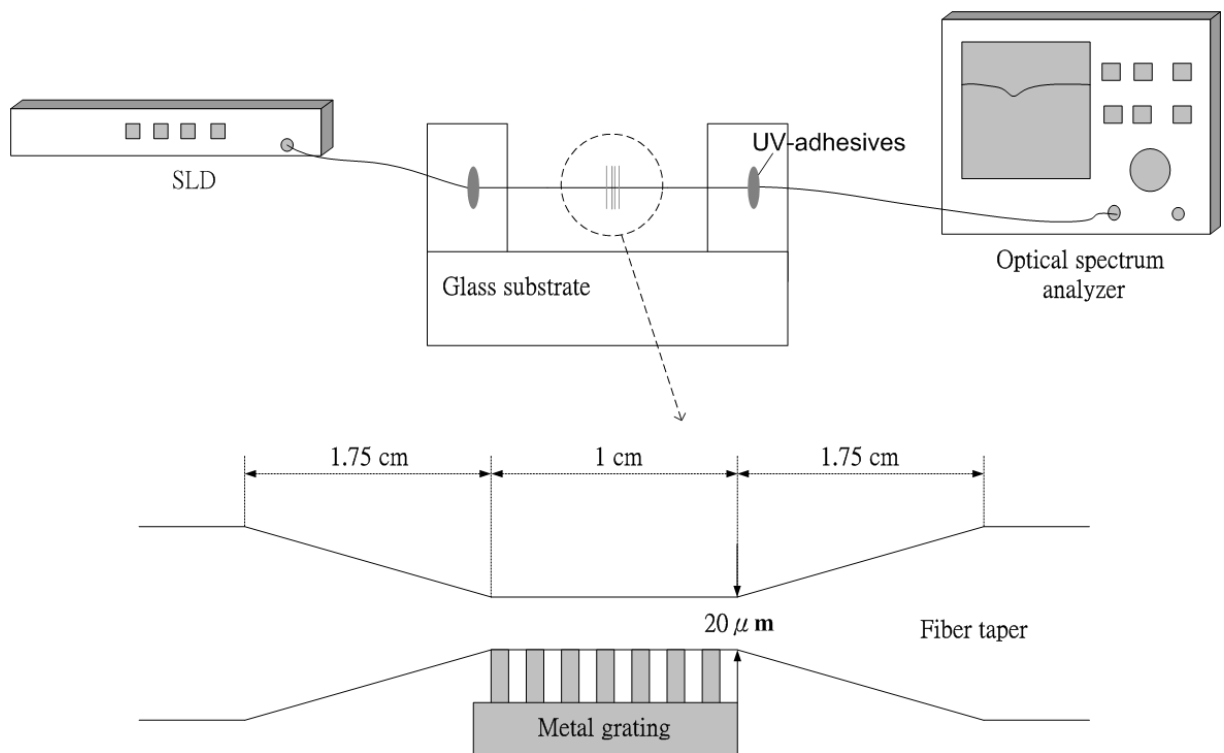


Fig.3.5 Diagram of measurement setup and the long period fiber grating composed of a fiber taper and a side-contact metal grating.

The fiber taper is mounted by UV-adhesives on a glass substrate, and the metal grating mounted on the translation stage is moved to contact the underside of the fiber taper. A broadband white light source containing superluminescent diodes (SLD) spanning from 1250 to 1650 nm was launched into one end of the fiber taper for performing measurement. The other end of fiber taper is connected to an optical spectrum analyzer (OSA) for measuring transmission spectra.

In order to understand the behavior of mode coupling, we have measured the transmission spectra of LPFGs when the surrounding medium is air or water. In the latter case we immerse both the taper waist and the grating in water and confirm that they are totally covered by the water. Fig.3.6 (a)-(d) shows the measured transmission spectra with different grating periods.





In Fig.3.6 (a), the resonant wavelengths of the LPFG with diameter of taper waist being  $20\mu\text{m}$ , and the grating period being  $421\mu\text{m}$  are  $1392\text{nm}$  and  $1532\text{nm}$ . The surrounding medium is air. Comparing with the case when the surrounding medium is water ( $1289\text{nm}$ ,  $1451\text{nm}$ , and  $1599\text{nm}$ ), the loss peaks shift to longer wavelengths by  $59\text{nm}$  and  $67\text{nm}$  respectively.

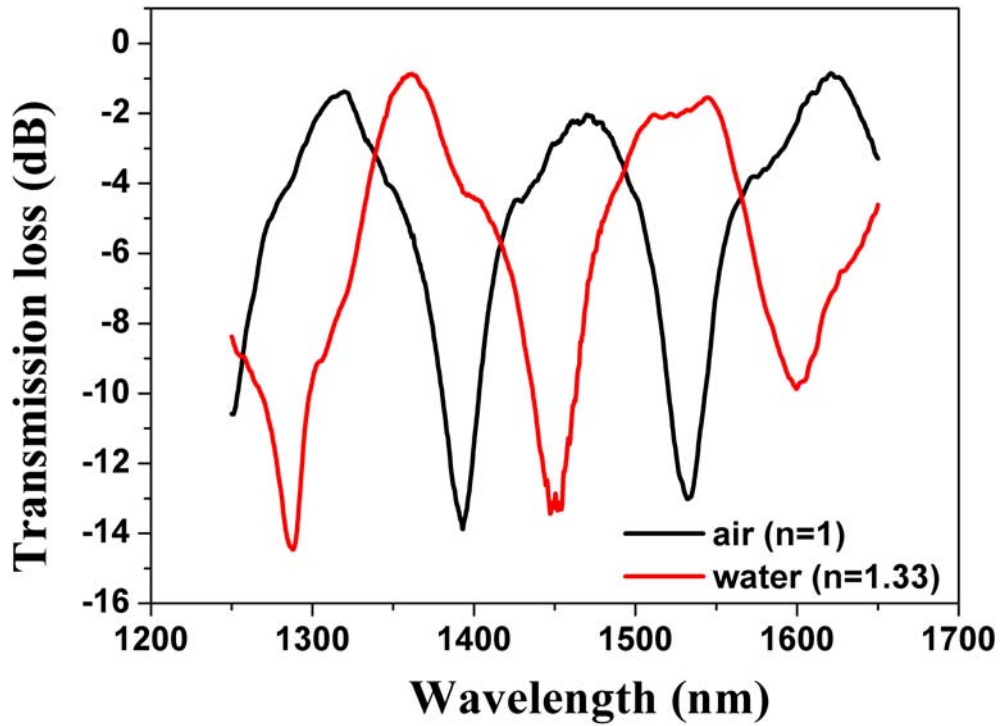


Fig.3.6(a) Transmission spectra of the LPFG with diameter of taper waist being  $20\mu\text{m}$ , grating period being  $421\mu\text{m}$ , and the surrounding medium being air (black line) and water (red line).

In Fig.3.6 (b), the resonant wavelengths of the LPFG with diameter of taper waist being  $20\mu\text{m}$ , and the grating period is  $430\mu\text{m}$ , are  $1327\text{nm}$  and  $1472\text{nm}$ . The surrounding medium is air. Comparing with the resonant wavelengths with the surrounding medium being water ( $1384\text{nm}$  and  $1558\text{nm}$ ), the loss peaks shift to longer wavelengths by  $57\text{nm}$  and  $86\text{nm}$  respectively.

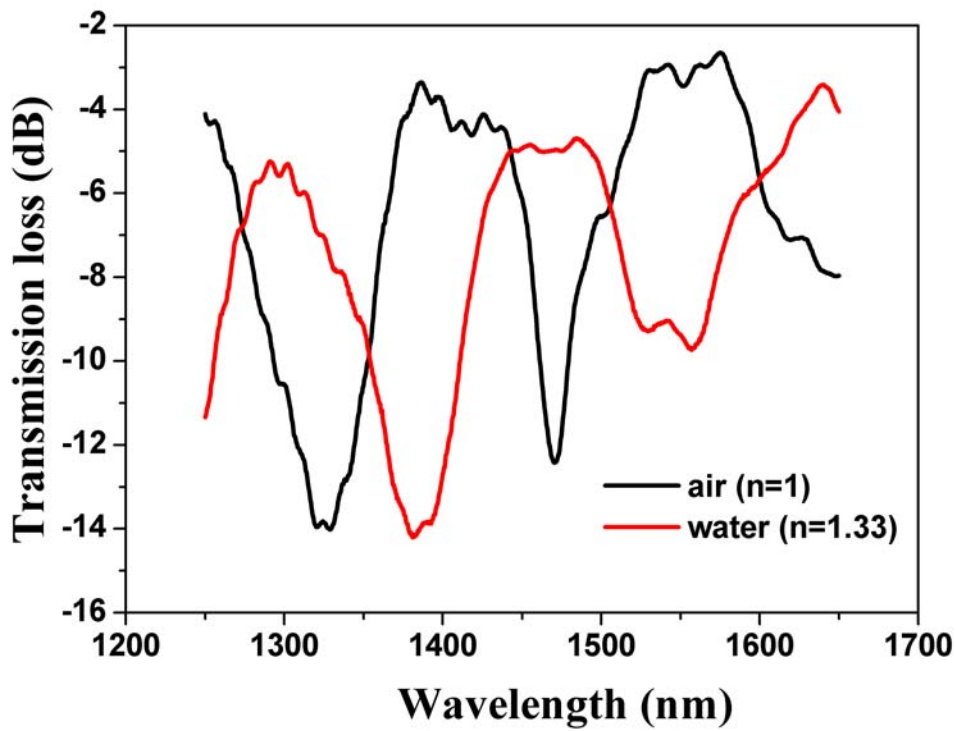


Fig.3.6(b) Transmission spectra of the LPFG with diameter of taper waist being  $20\mu\text{m}$ , grating period being  $430\mu\text{m}$ . The surrounding medium is air (black line) or water (red line).

In Fig.3.6 (c), the resonant wavelengths of the LPFG with diameter of taper waist being  $20\mu\text{m}$ , and the grating period being  $500\mu\text{m}$  are  $1255\text{nm}$ ,  $1401\text{nm}$  and  $1540\text{nm}$ . The surrounding medium is air. Comparing with the resonant wavelengths when the surrounding medium is water ( $1309\text{nm}$ ,  $1467\text{nm}$  and  $1638\text{nm}$ ), the loss peak shifts to longer wavelengths by  $54\text{nm}$ ,  $66\text{nm}$ , and  $98\text{nm}$  respectively.

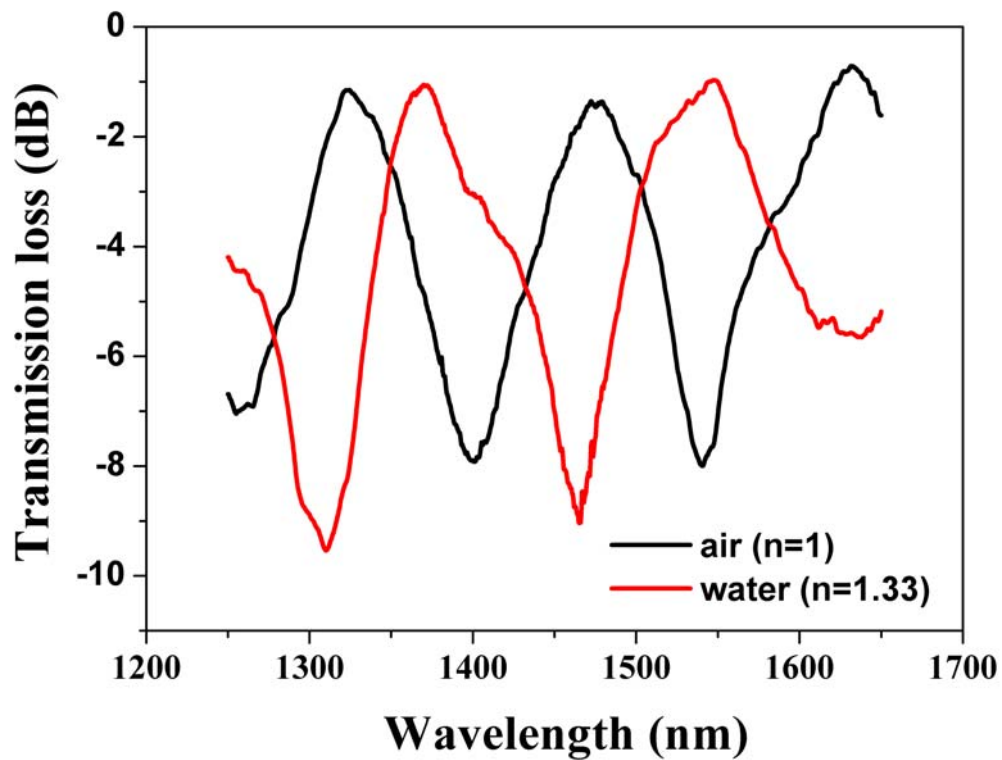


Fig.3.6(c) Transmission spectra of the LPFG with diameter of taper waist being  $20\mu\text{m}$ , grating period being  $500\mu\text{m}$ . The surrounding medium is air (black line) or water (red line).

From the above measurement results, we can conclude that the resonant wavelengths shift to longer wavelengths as the surrounding medium changes from air ( $n=1$ ) to water ( $n=1.33$ ). The tendency is different from the conventional LPFGs where the resonant wavelengths shift toward shorter wavelength as the refractive index of the surrounding medium increases. In the case of conventional LPFGs, the effective index of the core mode is almost constant and the effective indices of cladding modes increase as surrounding index increases, and therefore the index difference between core and cladding modes decreases for larger surrounding indices.

In the similar way, the index difference of two cladding modes in a fiber taper is smaller in water than in air-surrounding at the same wavelength. In order to match the difference of propagation constants through the same grating, the phase-matching wavelengths become shorter in a standard single-mode fiber and larger in a fiber taper for higher surrounding indices.

The amount of the shifted wavelength by changing the surrounding index is larger in the longer resonant wavelengths than in the shorter resonant wavelengths. This is because that the mode field extended to the surrounding medium is wider with longer wavelengths than with shorter wavelengths. Therefore, the longer resonant wavelength is more sensitive to the surrounding medium as compared with the shorter resonant wavelengths.

In Fig.3.6 (d), we compared the transmission spectra of LPFGs with different grating periods in air, which are  $421\mu\text{m}$  and  $430\mu\text{m}$  respectively. For coupling with same modes, the

loss peaks shift toward shorter wavelengths by  $65\mu\text{m}$  and  $60\mu\text{m}$  as the grating period changes from  $421\mu\text{m}$  to  $430\mu\text{m}$ . The tendency is different from the conventional LPFGs. The phase-matching wavelengths shift toward longer wavelengths as the grating period increases. This is caused by the different dispersion characteristics of the dispersion relations of a standard single mode fiber and a fiber taper, as we have already discussed in Chapter.2.

From the measured transmission spectra, we can see that the  $-3\text{dB}$  bandwidth is around  $100\text{nm}$ , which is larger compared to the bandwidth several  $\text{nm}$  in conventional LPFGs. The reason is that the changes in effective index difference with wavelength is not as obvious in a fiber taper when compared with the case in a standard single-mode fiber, as has been shown

in Fig. 2.13.

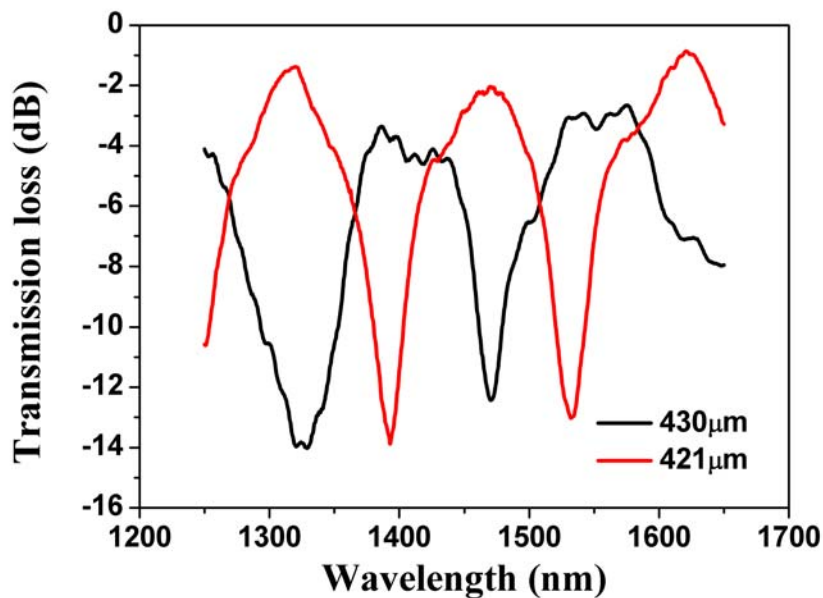
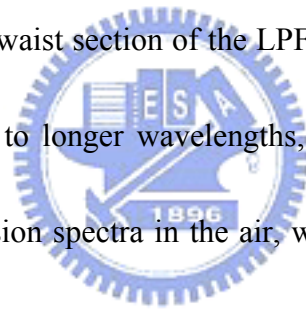


Fig.3.6(d) Transmission spectra of the LPFGs. The diameter of taper waist is  $20\mu\text{m}$ , grating period is  $430\mu\text{m}$ (black line),  $421\mu\text{m}$  (red line), and the surrounding medium is air.

### 3.3 Environment effects and applications

Environmental changes including the temperature and the surrounding medium may affect the grating period and properties of modes in LPFGs. Resonant wavelengths will shift in order to satisfy the phase-matching condition in (2.11). Therefore we can apply this property of LPFGs to make temperature sensors and index sensors. We have made the following measurements to test the environmental sensibility of our LPFGs.

The experimental transmission spectra of the LPFG device at room temperature in the air with the metal grating pitch of 436  $\mu\text{m}$  is shown in Fig. 3.7. When the water or alcohol are applied to cover the uniform waist section of the LPFGs, the two adjacent transmission dips gradually grow up and shift to longer wavelengths, as shown in Fig. 3.7. The black line indicates the LPFG transmission spectra in the air, while the blue and red lines present the LPFG transmission spectra with the uniform waist region immersed in the water and the alcohol, respectively. With the refractive index of the environmental material increased from water ( $n=1.33$ ) to alcohol ( $n=1.36$ ), the transmission dips shift to longer wavelength, and the sensitivity  $d\lambda/dn = 640 \text{ nm}$  and  $773 \text{ nm}$  for the first and second dips respectively.



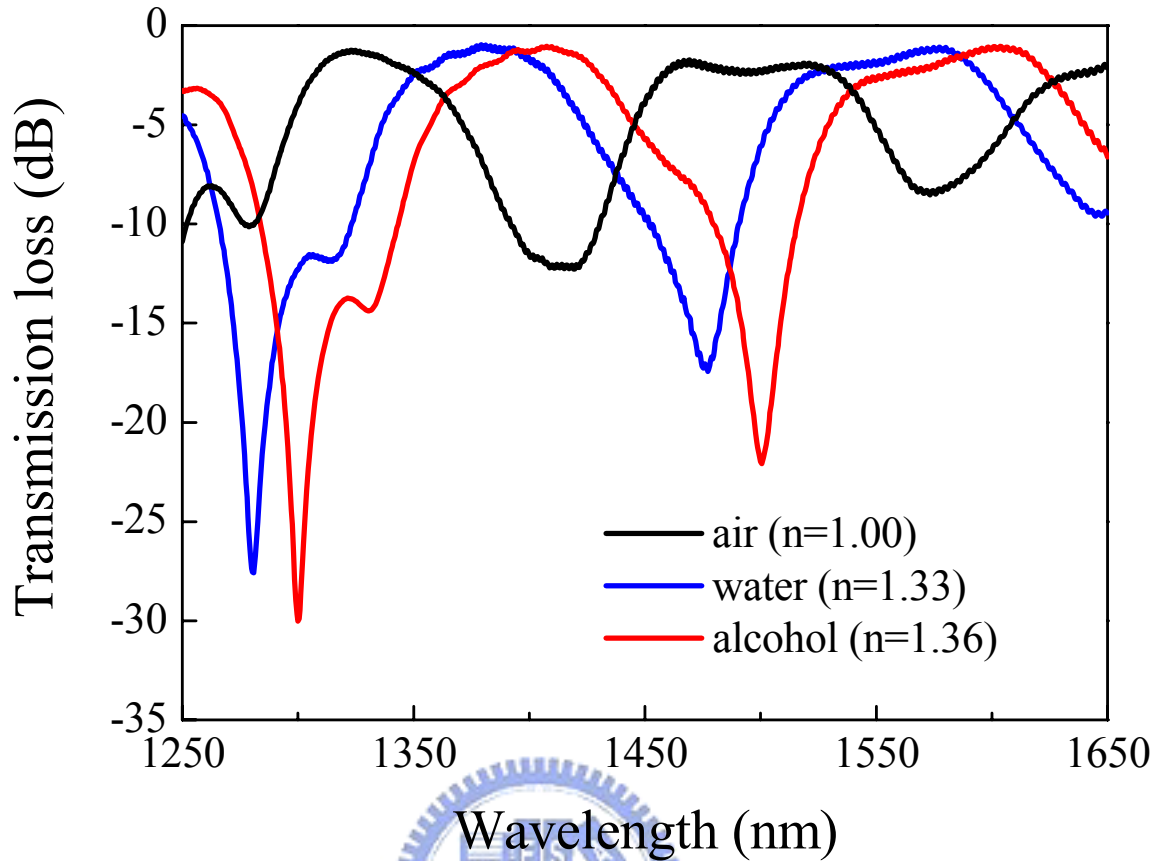


Fig. 3.7 Transmission spectra of the LPFGs with  $D = 20\mu\text{m}$ , grating period =  $436\mu\text{m}$ , and the surrounding medium is air (black line), water (blue line) and alcohol (red line).

Compare to the LPFG devices with the same surrounding medium reported in [3-4], our proposed LPFGs not only have superior index sensing characteristics but also have opposite wavelength shift tendency with respect to the increasing refractive index of surrounding medium. The attenuation dips increase when the refractive index of the environmental material increases. The modes spread out of the taper region in the LPFGs surrounded by the optical liquids much more than the case of being surrounded by the air, so the overlap among the fundamental mode, higher order modes, and the grating is improved. In this way the peak attenuation is increased and the environmental sensitivity of the phase-matching

wavelengths is enhanced.

To investigate the spectral responses of the LPFG at different heating temperatures, a metal grating with the period of 204  $\mu\text{m}$  is employed to form the device. The applied temperature  $T$  ranges from 25°C to 75°C, and the spectral responses are shown in Fig. 3.8.

The phase-matching wavelength moves to the shorter wavelength side and the peak attenuation gradually increased with increasing  $T$ . The grating pitch increases with increasing  $T$  in conventional LPFGs, and the phase-matching wavelength is changed to longer wavelengths. In this case the tuning efficiency substantially depends on the thermal expansion coefficient of the fiber material. However, the presently proposed LPFGs have decreasing resonance wavelength with respect to the increasing temperature, and the average temperature tuning efficiency  $\eta$  is estimated to be about -0.24 nm/ °C, which is greatly improved when compared to that of conventional LPFGs (around +0.06 nm/ °C [3-5]). The opposite temperature tuning tendency of the attenuation dip wavelength of the proposed LPFGs is due to the dispersion-engineered waveguiding structure that cause highly temperature-dependent dispersion characteristics between the coupling modes.

In contrast to the temperature tuning efficiency of the proposed LPFGs in the air, an optical liquid (Cargille index-matching liquids with the index  $n = 1.42$  at 1.46  $\mu\text{m}$  and the thermo-optic coefficient  $dn/dT = -3.74 \times 10^{-4} / ^\circ\text{C}$ ) is applied to cover the uniform tapered section and the metal grating to observe the temperature tuning efficiency with different



surrounding media. Figure 3.9 shows the wavelength shift of the LPFG with varying  $T$  surrounded by the optical liquids. From 25°C to 70°C, the phase-matching wavelength moves toward shorter wavelengths with increasing  $T$ . The optical liquid has a large thermo-optic coefficient than that of the air and the stannum, and the decreasing external refractive index makes  $n_{eff}$  decrease and the refractive index difference increase. Thus the phase-matching wavelength shift in Fig. 3.9 is larger than that of Fig. 3.8. This is a result due to the high thermo-optic coefficient of the optical liquid.

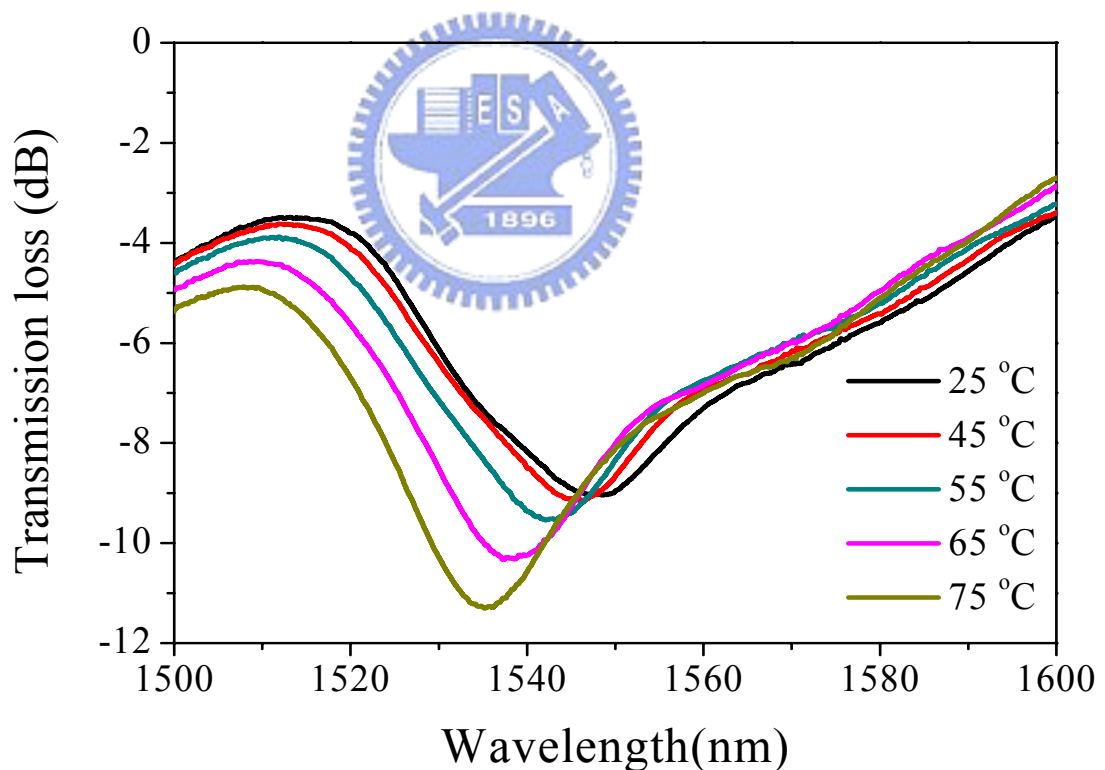


Fig. 3.8 Transmission spectra of the LPFGs in the air at different temperatures with  $D = 20\mu\text{m}$ , grating period = 204  $\mu\text{m}$ .

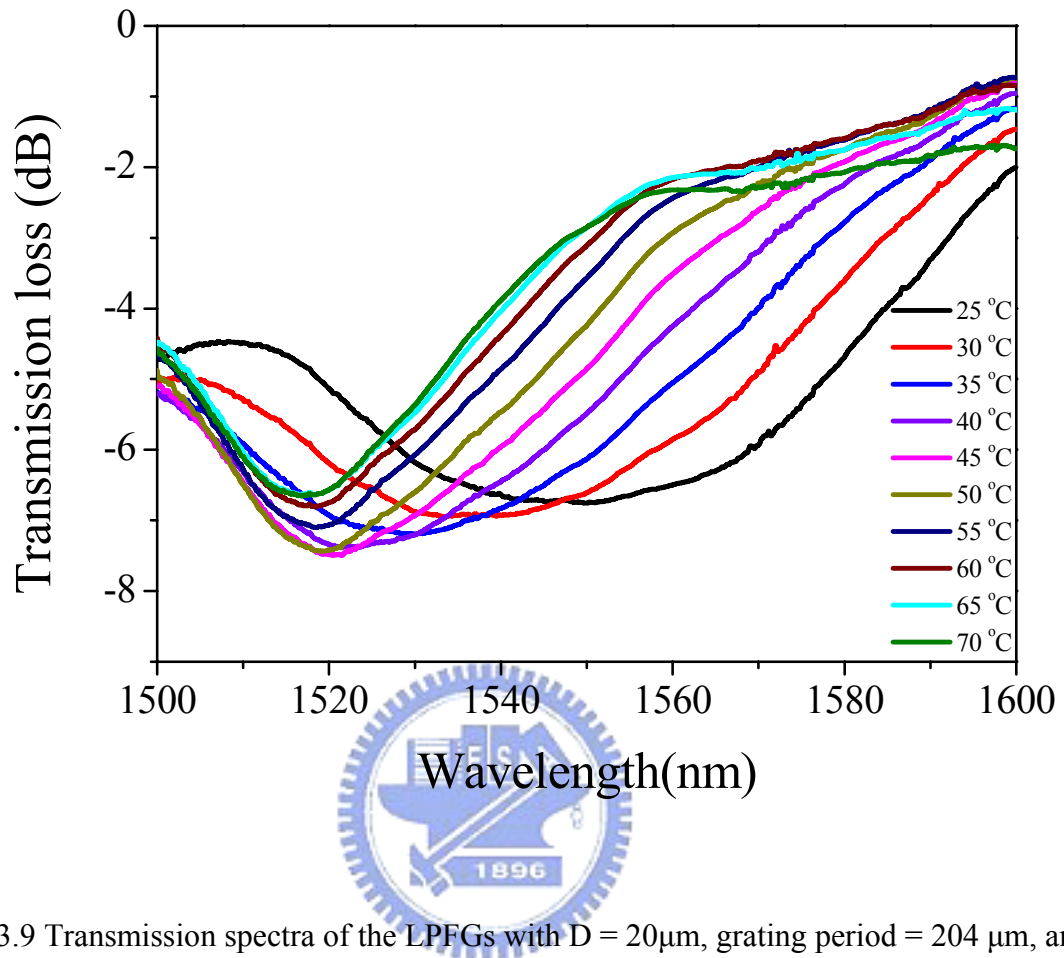


Fig. 3.9 Transmission spectra of the LPFGs with  $D = 20\mu\text{m}$ , grating period =  $204\mu\text{m}$ , and the surrounding medium is the heated Cargille index-matching liquids with the index  $n_D = 1.43$  at room temperature.

### 3.4 References

- [3-1] F. Bilodeau, K. O. Hill, S. Faucher, and D. C. Johnson, "Low-loss highly overcoupled fused couplers: Fabrication and sensitivity to external pressure." J. Lightwave Techno., vol. 6, pp.113-119,1988
- [3-2] V. Seidemann, S. Butefisch and S. Buttgenbach, "Fabrication and investigation of

in-plane compliant SU8 structures for MEMS and their application to micro valves and micro grippers,” *Sens. Actuators A* 97–98 , pp. 457–461, 2002.

[3-3] H. Ito, *IBM J. Res. Dev*, vol. 41, pp.69-81, 1997

[3-4] T. Zhu, Y. J. Rao, J. L. Wang and Y. Song, “A highly sensitive fiber-optic refractive index sensor based on an edge-written long-period fiber grating,” *IEEE Photon. Technol. Lett.* vol.19, no.24, pp.1946-1948, 2007.

[3-5] J. A. Besley, T. Wang, and L. Reekie, “Fiber cladding mode sensitivity characterization for long-period gratings,” *J. Lightwave Technol.*, vol.21, no.3, pp.848-853, 2003.



# Chapter 4.

## Conclusions

In conclusion, we have demonstrated a simple LPFG structure based on a tapered fiber with a side-contacted metal grating to form a flexible and high-sensitivity sensing device. The average temperature tuning efficiency  $\eta$  is estimated to be about  $-0.24 \text{ nm/ } ^\circ\text{C}$ , which is greatly improved when compared to that of conventional LPFGs (around  $+0.06 \text{ nm/ } ^\circ\text{C}$ ). In particular, we have observed that there are two different spectral responses compared to conventional LPFGs. The first one is the un-usual spectral response of decreasing phase-matching wavelength with respect to the increasing grating period. The other is the tendency of increasing phase-matching wavelength with respect to the increasing surrounding index. The unusual spectral responses are caused by the different characteristics of intermodal dispersion in standard SMFs and fiber tapers, as we have illustrated theoretically in Chapter 2. In future work, the temperature/index tuning sensitivity can definitely be improved by employing material and waveguide dispersion engineering. There are many physical parameters can be optimized: diameter of fiber tapers, surrounding index, length of grating, grating structure and grating materials. It should be possible to further improve the tuning sensitivity of these LPFG devices.